GABAergic neuron-to-glioma synapses in diffuse midline gliomas

Tara Barron[1], Belgin Yalçın[1], Aaron Mochizuki[1], Evan Cantor[2], Kiarash Shamardani[1], Dana Tlais[1], Andrea Franson[2], Samantha Lyons[2], Vilina Mehta[1], Samin Maleki Jahan[1], Kathryn R. Taylor[1], Michael B. Keough[1], Haojun Xu[1], Minhui Su[1], Michael A. Quezada[1], Pamelyn J Woo[1], Paul G. Fisher[1], Cynthia J. Campen[1], Sonia Partap[1], Carl Koschmann[2], Michelle Monje[1,3,*]

1 Department of Neurology and Neurological Sciences, Stanford University, Stanford CA 94305 USA

2 Department of Pediatric Hematology/Oncology, University of Michigan, Ann Arbor Michigan USA

3 Howard Hughes Medical Institute, Stanford University, Stanford CA 94305 USA

*Please send correspondence to: Michelle Monje MD PhD (mmonje@stanford.edu)

Abstract

Pediatric high-grade gliomas are the leading cause of brain cancer-related death in children. High-grade gliomas include clinically and molecularly distinct subtypes that stratify by anatomical location into diffuse midline gliomas (DMG) such as diffuse intrinsic pontine glioma (DIPG) and hemispheric high-grade gliomas. Neuronal activity drives high-grade glioma progression both through paracrine signaling[1,2] and direct neuron-to-glioma synapses[3-5]. Glutamatergic, AMPA receptor-dependent synapses between neurons and malignant glioma cells have been demonstrated in both pediatric[3] and adult high-grade gliomas[4], but neuron-to-glioma synapses mediated by other neurotransmitters remain largely unexplored. Using whole-cell patch clamp electrophysiology, *in vivo* optogenetics and patient-derived glioma xenograft models, we have now identified functional, tumor-promoting GABAergic neuron-to-glioma synapses mediated by $GABA_A$ receptors in DMGs. GABAergic input has a depolarizing effect on DMG cells due to NKCC1 expression and consequently elevated intracellular chloride concentration in DMG tumor cells. As membrane depolarization increases glioma proliferation[3], we find that the activity of GABAergic interneurons promotes DMG proliferation *in vivo*. Increasing GABA signaling with the benzodiazepine lorazepam – a positive allosteric modulator of $GABA_A$ receptors commonly administered to children with DMG for nausea or anxiety - increases $GABA_A$ receptor conductance and increases glioma proliferation in orthotopic xenograft models of DMG. Conversely, levetiracetam, an anti-epileptic drug that attenuates GABAergic neuron-to-glioma synaptic currents, reduces glioma proliferation in patient-derived DMG xenografts and extends survival of mice bearing DMG xenografts. Concordant with gene expression patterns of $GABA_A$ receptor subunit genes across subtypes of glioma, depolarizing GABAergic currents were not found in hemispheric high-grade gliomas. Accordingly, neither lorazepam nor levetiracetam influenced the growth rate of hemispheric high-grade glioma patient-derived xenograft models. Retrospective real-world clinical data are consistent with these conclusions and should be replicated in future prospective clinical studies. Taken together, these findings uncover GABAergic synaptic communication between GABAergic interneurons and diffuse midline glioma cells, underscoring a tumor subtype-specific mechanism of brain cancer neurophysiology with important potential implications for commonly used drugs in this disease context.

Introduction

Diffuse midline glioma (DMG), which occurs most commonly in the brainstem and is also known as diffuse intrinsic pontine glioma (DIPG), is a lethal childhood central nervous system cancer with few therapeutic options and a median survival of only 10-13 months[6,7]. The majority of DMGs exhibit a mutation in genes encoding histone H3 (H3K27M), and occur in the brainstem, thalamus and spinal cord[8-10]. Multiple lines of evidence support

the concept that DMG originates from oligodendroglial lineage precursor cells[11-15]. During postnatal development and adulthood, oligodendroglial precursor cells (OPCs) communicate with neurons through both paracrine factor signaling[16-18] and through glutamatergic and GABAergic neuron-to-OPC synapses[19-23]; oligodendroglial precursor cell proliferation is robustly regulated by neuronal activity[24]. Similar to these effects on their normal cellular counterparts, glutamatergic neuronal activity drives the proliferation and growth of DMG and other high-grade[1,4,25,26] and low-grade[2] gliomas. The mechanisms by which neuronal activity promotes glioma progression include activity-regulated paracrine factor secretion[1,2,25,26] as well as electrochemical communication through AMPA (α-amino-3-hydroxy-5-methyl-4-isoxazole propionic acid) receptor (AMPAR)-mediated neuron-to-glioma synapses[3,4] and activity-dependent, potassium-evoked glioma currents that are evident in both pediatric and adult forms of high-grade gliomas[3,4]. Depolarizing current alone is sufficient to drive malignant glioma growth in orthotopic xenograft models [3], underscoring the need for a comprehensive understanding of electrochemical mechanisms that enable glioma membrane depolarization in each molecularly distinct form of glioma. Here, we explore whether GABAergic synapses exist between GABAergic interneurons and DMG cells and test the hypothesis that putative GABAergic synaptic signaling is depolarizing and promotes tumor progression in H3K27M-altered DMG.

Results

$GABA_A$ receptor and postsynaptic gene expression in DMG

To determine whether genes involved in GABAergic synaptic transmission are expressed in high-grade gliomas, we analyzed single-cell RNAseq datasets from primary patient tumor samples of H3K27M+ DMG cells, IDH wild-type (WT) hemispheric high-grade glioma cells, IDH mutant (mut) hemispheric high-grade glioma cells, and tumor-associated non-malignant oligodendrocytes (OLs). H3K27M+ DMG cells broadly expressed $GABA_A$ receptor subunit genes, including α and β subunits, as well as ARHGEF9, GPHN, and NLGN2, which are associated with GABAergic post-synaptic regions (Figure 1a). These genes were expressed to a much greater extent in H3K27M+ DMG cells than in IDH WT high-grade gliomas (Figure 1a).

Functional GABAergic neuron-glioma synapses

To determine whether putative functional GABAergic neuron-glioma synapses exist, we performed electrophysiological recordings from xenografted H3K27M+ DMG cells in response to stimulation of local GABAergic interneurons. Green fluorescent protein (GFP)-expressing glioma cells were xenografted into the CA1 region of the hippocampus, a well-defined circuit in which neuron-to-glioma synapses have been previously reported[3] and allowed to engraft and grow for at least 8 weeks. Acute hippocampal sections were prepared from these mice, and DMG cell responses to electrical stimulation of local neurons with a bipolar stimulator were recorded using whole-cell patch clamp electrophysiology (Figure 1b). Using a high Cl^- internal solution and in the presence of AMPAR antagonist NBQX (2,3-dihydroxy-6-nitro-7-sulfamoyl-benzo[f]quinoxaline) to inhibit AMPAR-mediated currents, local stimulation led to an inward current in DMG cells recorded in voltage clamp (Figure 1c). This current was

blocked with perfusion of picrotoxin (PTX), a $GABA_A$ receptor inhibitor, indicating that these synaptic currents are mediated by GABA. GABAergic neuron-to-glioma synapses were observed in two distinct patient-derived xenograft models (Figure 1d). Cells were filled with Alexa Fluor 568 dye during electrophysiological recording and then slices were post-fixed, immunostained for tumor cell markers [GFP and human nuclear antigen (HNA)] and imaged on a confocal microscope to confirm that the cells recorded from were glioma cells (Figure 1e).

GABA depolarizes DMG cells due to NKCC1-mediated high intracellular Cl^-

$GABA_A$ receptor activation can either depolarize or hyperpolarize a cell, depending on the intracellular Cl^- concentration. In mature neurons, Cl^- concentration is low, leading to an influx of Cl^- through $GABA_A$ receptors and thus, hyperpolarization [27]. OPCs exhibit a high intracellular Cl^- concentration, leading to an efflux of Cl^- through $GABA_A$ receptors, and thus GABAergic neuron-to-OPC synapses cause depolarization[20]. Perforated patch recordings of xenografted H3K27M+ DMG cells using gramicidin-A revealed that local application of GABA induced an inward current in voltage clamp and corresponding depolarization in current clamp (Figure 2a-b). The effect of local GABA application on H3/IDH WT pediatric hemispheric glioblastoma (pGBM) was negligible in comparison (Figure 2a-b). PTX inhibited the current and depolarization in response to GABA application, indicating that $GABA_A$ receptors are responsible for this depolarizing effect. To determine the reversal potential of $GABA_A$ currents (E_{GABA}) in H3K27M+ DMG and H3/IDH WT pGBM xenografts, we recorded response to local GABA application at varying holding potentials (Figure 2c). The currents in response to GABA were plotted against the

holding potentials, and E_{GABA} was found to be -19.61 ± 8.29 mV and -14.14 ± 9.04 mV for H3K27M+ DMG cells from two different patient-derived models (SU-DIPGVI and SU-DIPGXIII-FL, respectively) and -47.44 ± 7.79 mV for H3/IDH WT pGBM (Figure 2d; Extended Data Figure 1). Using these reversal potentials to calculate the intracellular Cl^- concentration of each glioma type, we find the intracellular Cl^- concentration of H3K27M+ DMG cells to be 62.65 mM in SU-DIPGVI cells and 76.88 mM in SU-DIPGXIII-FL cells, and that of H3/IDH WT pGBM to be 22.12 mM. During whole-cell recordings with high Cl^- internal solution, the reversal potential was -0.41 ± 12.98 mV in H3K27M+ DMG cells, illustrating the critical role of chloride concentration gradients.

Cation–chloride cotransporters, such as the Na-K-Cl cotransporter NKCC1, have an important role in setting intracellular Cl^- concentration. *SLC12A2*, the gene that encodes for NKCC1, is expressed in H3K27M+ DMG (Figure 2e). To determine the role of NKCC1 in E_{GABA} in DMG cells, we used perforated patch to record the response to local GABA application in the presence of bumetanide, an NKCC1 inhibitor. After bath perfusion of bumetanide, E_{GABA} was shifted from -19.61 ± 8.29 mV to -54.20 ± 8.19 mV in H3K27M+ DMG cells (Figure 2f), a value similar to that found in H3/IDH WT pGBM cells (Figure 2d) indicating that NKCC1 function is critical for the depolarizing effect of GABA on these cells.

GABAergic interneurons increase DMG proliferation

Past work has demonstrated that glutamatergic neuronal activity promotes glioma progression[1-5], and that depolarization of glioma cells plays a central role in these effects of neuronal activity on glioma proliferation[3]. Since GABA has a depolarizing effect on

DMG cells as described above, we sought to determine whether GABAergic interneurons drive DMG proliferation through depolarizing GABAergic synaptic input. We first used whole-cell patch clamp electrophysiology to confirm that we could perform optogenetic and pharmacological targeting of GABAergic neuron-to-glioma synapses. We genetically expressed ChRmine, a red-shifted channelrhodopsin[28], in Dlx-expressing GABAergic interneurons in the CA1 region of the hippocampus and recorded the response of xenografted glioma cells to 5 ms optogenetic stimulation of those neurons (Figure 3a). PTX-sensitive GABAergic post-synaptic currents in DMG cells were observed in response to optogenetic interneuron stimulation (Figure 3b). We also observed the tetrodotoxin (TTX)-sensitive prolonged currents, evoked by activity-dependent extracellular K^+ increase, that we have previously described[3] (Figure 3b). Whole cell patch clamp recordings of Dlx-ChRmine-expressing interneurons confirmed that optogenetic stimulation evoked depolarization (Extended Data Figure 2a). Pharmacological targeting of GABAergic neuron-to-glioma synaptic input using a benzodiazepine, lorazepam, which increases conductance of $GABA_A$ receptors, increased the amplitude of GABAergic post-synaptic currents in DMG cells (Figure 3c-e).

We next sought to test the effect of interneuron activity and GABAergic synaptic input into DMG cells *in vivo*. Dlx-ChRmine was expressed in hippocampal interneurons via AAV viral vector injection to the CA1 region, and *in vivo* optogenetic stimulation of interneuron activity was confirmed by expression of the immediate early gene cFos (Extended Data Figure 2b). Eleven weeks after injection of Dlx-ChRmine vector into the hippocampus, and eight weeks after xenografting patient-derived H3K27M+ DMG cells to the same area, the CA1 region of the hippocampus was optogenetically stimulated

(595 nm light, 40 Hz, 30 sec on/90 sec off over 30 minutes) in awake, behaving mice to stimulate GABAergic interneuron activity (Figure 3f). Control mice were identically manipulated, but light was not delivered during mock optogenetic stimulation. The thymidine analogue EdU was administered systemically to mice at the time of optogenetic or mock stimulation to label proliferating cells, and glioma cell proliferation was analyzed 24-hours later. *In vivo* optogenetic stimulation of GABAergic interneurons promoted proliferation of xenografted DMG cells (Figure 3g). Similarly, treatment of xenografted mice with lorazepam, which increases $GABA_A$ receptor signaling, exerted a dose-dependent proliferative effect on H3K27M+ DMG in each of three independent patient-derived orthotopic xenograft models (Figure 3h-j). While the effect of lorazepam was most robust at high doses (8 mg/kg), in each xenograft model a significant dose-dependency was evident with ANOVA post-test for linear contrast. The microenvironment of the brain, such as the presence of GABAergic neurons, is required for the proliferative effect of lorazepam, as no effect of lorazepam was observed in H3K27M+ DMG monocultures (Extended Data Figure 3a). As expected, given the lack of GABA-induced currents in H3/IDH WT gliomas, lorazepam did not increase glioma proliferation in mice bearing patient-derived H3/IDH WT pGBM xenografts (Extended Data Figure 4).

Therapeutic potential of targeting GABAergic neuron-glioma synapses

As neuron-glioma synapses robustly promote glioma cell proliferation and tumor progression, identifying pharmacological treatments that target these synapses has high therapeutic potential. Levetiracetam, a generally well-tolerated anti-epileptic drug with multiple mechanisms of action, reduces GABAergic post-synaptic currents in DMG cells

(Figure 4a-b). Strikingly, mice bearing H3K27M+ DMG xenografts treated with levetiracetam exhibited longer survival than vehicle-treated controls (Figure 4c). Levetiracetam treatment decreased glioma proliferation in mice bearing H3K27M+ DMG xenografts compared to vehicle-treated controls, an effect observed in three independent patient-derived orthotopic xenograft models of H3K27M+ DMG (Figure 4d-f). The effect of levetiracetam on glioma proliferation is dependent on the brain microenvironment rather than cell-intrinsic effects, as no effect of levetiracetam was observed in H3K27M+ DMG monocultures (Extended Data Figure 3b).

Retrospective, real-world data from two major US pediatric neuro-oncology centers (Stanford University and University of Michigan) was assessed to query possible effects of levetiracetam on overall survival in pediatric patients with high-grade gliomas. Kaplan-Meier analysis of all pHGG patients (n = 216) suggests a survival advantage of levetiracetam usage (Extended Data Figure 5a). For multivariable survival analysis, we utilized an elastic net-regularized Cox regression for variable selection and found that in all patients with high-grade glioma, a diagnosis of DMG was – as expected - associated with decreased overall survival (coefficient +0.55), and that thalamic DMG tumor location (coefficient -0.20), and levetiracetam (coefficient -0.11) were associated with increased overall survival; the variables of age, sex, ONC201 usage, and panobinostat usage had coefficients of zero. Conventional or targeted chemotherapy other than ONC201 and panobinostat were surprisingly associated with increased overall survival (coefficient -0.61), which may be explained by the observation that pontine DMG subjects in the historical database often did not receive any conventional or targeted therapy (Extended Data Table 1) due to demonstrated lack of efficacy of conventional chemotherapy in

pontine DMG[29]. Hypothesizing that DMGs drove the positive survival association of levetiracetam usage, we next evaluated DMG and hemispheric HGGs separately. These databases include subjects with biopsy-demonstrated H3K27M-mutated or H3WT diffuse midline gliomas as well as subjects prior to availability of molecular testing for whom diagnosis was based only on the typical radiographic appearance of DMGs; both H3K27M-altered and H3WT subgroups of DMGs are therefore included (Extended Data Table 1). The DMG analysis suggests that patients with DMG who had a history of levetiracetam usage (n = 15 children) exhibited a longer median overall survival (OS) compared to those without levetiracetam usage (n = 105 children; Extended Data Figure 5b, Extended Data Table 1). Those DMG patients with a history of levetiracetam usage had a median OS of 20.3 months, compared to those without levetiracetam usage who exhibited a median OS of 9.2 months (P=0.025). Of note, thalamic DMG represented a higher proportion of the group with a history of levetiracetam usage than the group with no history of levetiracetam usage. Comparing subjects with thalamic and pontine DMG who received levetiracetam, we find no difference in OS in this levetiracetam usage group (Extended Data Figure 5c), suggesting that the higher proportion of thalamic DMG in this group does not account for the observed increased median OS compared to the group without levetiracetam usage. The median OS of the control (no levetiracetam usage) group is consistent with the expected median OS for DIPG/DMG (10-11 months for pontine DMG, 13 months for thalamic DMG)[6,7]. Important caveats are that these data are retrospective, the numbers are small, and levetiracetam should be studied in future prospective clinical studies with stratification by molecular subtype and DMG location before drawing conclusions.

In contrast to the anti-proliferative effect of levetiracetam on xenografted H3K27M+ DIPG/DMG, levetiracetam treatment did not significantly affect glioma proliferation in mice bearing patient-derived hemispheric (H3/IDH WT) high-grade glioma xenografts in three independent models of pediatric and adult hemispheric H3/IDH WT glioblastoma (Figure 4g-i). Concordantly, analysis of the retrospective clinical data focused on hemispheric pediatric high-grade gliomas revealed no effect of levetiracetam usage on OS in pediatric patients with non-DMG, hemispheric high-grade gliomas (n=37, median OS 24.6 months vs n=60 children, median OS 17.0 months with and without levetiracetam use, respectively, P=0.74, Extended Data Figure 5d, Extended Data Table 2).

Phenytoin and ethosuximide, antiepileptic drugs that reduce neuronal hyperexcitability but do not directly act on known mechanisms of neuron-to-glioma communication, do not influence DMG proliferation *in vivo* or *in vitro* (Extended Data Figure 6), highlighting the importance of specifically targeting neuron-to-glioma synapses.

Discussion

Glutamatergic neuronal activity has emerged as a powerful regulator of glioma progression[2-4,25,26,30]. Across multiple clinically and molecularly distinct forms of pediatric and adult gliomas, activity-regulated paracrine factors such as BDNF and shed neuroligin-3 promote glioma growth [1,2,25,30]. Similarly, AMPAR-mediated glutamatergic synapses drive progression in both H3K27M-altered DMG and hemispheric (H3/IDH WT) glioblastomas[3,4]. Here, we demonstrate that GABAergic interneurons also promote glioma progression through GABAergic synapses that are depolarizing and growth-promoting in the specific disease context of diffuse midline gliomas. In contrast, only

minimal currents were found in the hemispheric (IDH/H3 WT) high-grade glioma models used here; it is possible that some subtypes of hemispheric glioma may be found to respond to GABA heterogenously[31]. We found that the commonly used anti-seizure drug levetiracetam attenuates these GABAergic currents in diffuse midline gliomas, through mechanisms that remain to be determined. Levetiracetam has multiple described mechanisms, including binding to SV2A to decrease presynaptic release, but whether this represents the mechanism operant in diminishing DMG GABA currents remains to be tested in future studies. These discoveries highlight the therapeutic potential of re-purposing levetiracetam to decrease GABAergic signaling in diffuse midline gliomas.

While this therapeutic potential is supported by the preclinical evidence and suggested by the retrospective clinical data presented here, it is important to note that prospective clinical trials are required to validate this effect. In this clinical retrospective study, it may be that those subjects who developed seizures and therefore received levetiracetam had tumors that are particularly neurotrophic and thus more susceptible to therapy with levetiracetam. It is also possible that tumors growing in neuroanatomical locations with relatively more GABAergic input or different GABA-dependent circuit dynamics are differentially affected by levetiracetam therapy. An unknown confounder could also be associated with levetiracetam therapy. Future work, studying larger numbers of patients and stratifying subjects based on DMG location, molecular characteristics, and glioma neuroscience correlative markers will be required to draw conclusions about the potential role of levetiracetam for DMG therapy.

The anti-seizure drugs tested were growth-inhibitory only if the drug targeted specific mechanisms of neuron-glioma interaction in that tumor type. Ethosuximide and phenytoin do not target known mechanisms of neuron-glioma interactions and did not affect tumor proliferation in the preclinical models used here. Similarly, neither levetiracetam nor lorazepam influenced the proliferation of the three independent hemispheric (H3/IDH WT) glioblastoma models used here. Past clinical studies of antiepileptic drug effects in adult high-grade glioma have not been guided by knowledge of drugs that specifically target neurophysiological mechanisms operant in that tumor type. Not surprisingly, the results of such anti-seizure medication studies have been mixed. Levetiracetam used concomitantly with chemoradiation has been reported to improve outcomes in hemispheric, H3/IDH WT glioblastoma in some studies [32], while large meta-analyses have found no discernable effect on outcome in others [33,34]. These discordant findings in the literature may reflect the heterogeneity inherent in hemispheric H3/IDH WT high-grade gliomas[34], and specific subgroups of H3/IDH WT glioblastoma yet-to-be determined could be responsive to levetiracetam. Here, we found no effect of levetiracetam in three independent preclinical models of pediatric and adult hemispheric (H3/IDH WT) high-grade glioma and no effect of levetiracetam in retrospective analyses of pediatric patients with non-DMG, hemispheric high-grade gliomas.

In DMGs, the risk to benefit ratio of benzodiazepines should be carefully considered. Benzodiazepines, which potentiate signaling through $GABA_A$ receptors, promote glioma GABAergic currents and tumor proliferation in the H3K27M-altered DMG models used here. Benzodiazepines are commonly used in children with DMG for nausea, anxiety,

claustrophobia during MRI scans and other medical procedures, and for other reasons. While benzodiazepines are important medications for palliative care, use should be carefully considered in DMG outside of the context of end-of-life care and should be further evaluated in clinical analyses. Conversely, and further underscoring differences between DMG and hemispheric high-grade gliomas, preclinical studies indicate that GABA and GABAergic interneurons may instead be growth-inhibitory hemispheric (H3/IDH WT) adult glioblastoma models[35,36]. These findings underscore the therapeutic importance of elucidating the neurophysiology of defined subtypes of brain cancers to identify the patient populations for which a particular neurophysiological drug may be beneficial or detrimental. Understanding the neuroscience of brain tumors will enable the development of effective and safe therapeutic approaches, incorporating neuroscience-informed therapies into combinatorial strategies targeting both cell-intrinsic and microenvironmental mechanisms that drive progression of these devastating cancers.

Methods

Human samples and data

For all human tissue and cell studies, informed consent was obtained, and tissue was used in accordance with protocols approved by the Stanford University Institutional Review Board (IRB). IRB approval was also obtained for retrospective analyses of real-world clinical data kept in IRB-approved databases at Stanford University and University Michigan.

Mice and housing conditions

All *in vivo* experiments were conducted in accordance with protocols approved by the Stanford University Institutional Animal Care and Use Committee (IACUC) and performed in accordance with institutional guidelines. Animals were housed according to standard guidelines with free access to food and water in a 12 h light:12 h dark cycle. For brain tumor xenograft experiments, the IACUC does not set a limit on maximal tumor volume but rather on indications of morbidity. In no experiments were these limits exceeded as mice were euthanized if they exhibited signs of neurological morbidity or if they lost 15% or more of their body weight.

Orthotopic xenografting

For all xenograft studies, NSG mice (NOD-SCID-IL2R gamma chain-deficient, The Jackson Laboratory) were used. Male and female mice were used equally. A single-cell suspension from cultured SU-DIPG-VI-GFP, SU-DIPG-XIII-FL-GFP, SU-DIPG-50-GFP, SU-pcGBM2-GFP, SF0232, or SF0238 neurospheres were prepared in sterile PBS immediately before the xenograft procedure. Animals at postnatal day (P) 28–30 were anaesthetized with 1–4% isoflurane and placed in a stereotactic apparatus. The cranium was exposed via midline incision under aseptic conditions. Approximately 300,000 cells in 3 µl sterile PBS were stereotactically implanted through a 26-gauge burr hole, using a digital pump at infusion rate of 0.4 µl min^{-1} and 26-gauge Hamilton syringe. For all electrophysiology and optogenetics experiments, cells were implanted into the CA1 region of the hippocampus (1.5 mm lateral to midline, -1.8 mm posterior to bregma, −1.4 mm deep to cranial surface). SU-DIPG-XIII-FL-GFP for lorazepam and levetiracetam treatments were xenografted into the premotor cortex (0.5 mm lateral to midline, 1.0 mm

anterior to bregma, −1.75 mm deep to cranial surface). SU-DIPG-XIII-P for survival study and SU-DIPG-VI-GFP and SU-DIPG-50-GFP for lorazepam, levetiracetam, ethosuximide, and phenytoin treatments were xenografted into the pons (1.0 mm lateral to midline, −0.8 mm posterior to lambda, −5.0 mm deep to cranial surface). At the completion of infusion, the syringe needle was allowed to remain in place for a minimum of 2 min, then manually withdrawn at a rate of 0.875 mm min^{-1} to minimize backflow of the injected cell suspension.

Patient-derived cell culture

All high-grade glioma cultures were generated as previously described [11]. In brief, tissue was obtained from high-grade glioma (WHO (World Health Organization) grade III or IV) tumors at the time of biopsy or from early post-mortem donations. Tissue was dissociated both mechanically and enzymatically and grown in a defined, serum-free medium designated 'tumor stem media' (TSM), consisting of neurobasal(-A) (Invitrogen), B27(-A) (Invitrogen), human bFGF (20 ng ml^{-1}; Shenandoah), human EGF (20 ng ml^{-1}; Shenandoah), human PDGF-AA (10 ng ml^{-1}) and PDGF-BB (10 ng ml−1; Shenandoah) and heparin (2 ng ml^{-1}; Stem Cell Technologies). For all patient-derived cultures, mycoplasma testing was routinely performed, and short tandem repeat DNA fingerprinting was performed every three months to verify authenticity. The short tandem repeat fingerprints and clinical characteristics for the patient-derived cultures and xenograft models used have been previously reported [37].

Single-cell sequencing analysis

We combined publicly available single-cell datasets processed and annotated previously[13,38], all sequenced using smart-seq2 protocol. Following the quality-control measures taken in these studies, we filtered the data to keep cells with more than 400 detected genes, and genes that were expressed in more than 3 cells. We assessed the single-cell transcriptome from 6,341 adult IDH-mutant glioma cells derived from biopsies from 10 study participants, 599 adult wild-type IDH glioma cells derived from biopsies from 3 study participants, and 2,458 pediatric H3K27M DMG cells derived from biopsies from 6 study participants, as well as the single-cell transcriptome of patient-derived SU-DIPGVI and SU-DIPGXIII-FL cells. Malignant cells were inferred by expression programs and detection of tumor-specific genetic alterations. For each sample, we performed first cell-level normalization, and then centered the gene expression around 0 to allow principal component analysis (PCA) computation. Following the PCA reduction, we clustered the cells using shared nearest neighbor clustering. To examine the various $GABA_A$ receptor signatures of each of the cells in each cluster, we used the function AddModuleScore by Seurat package, which calculates the average expression levels of the gene set subtracted by the aggregated expression of 100 randomly chosen control gene sets, where the control gene sets are chosen from matching 25 expression bins corresponding to the tested gene set expression. The gene sets used are as followed: $GABA_A$ receptor α: GABRA1, GABRA2, GABRA3, GABRA4, GABRA5, GABRA6; $GABA_A$ receptor β: GABRB1, GABRB2, GABRB3; total $GABA_A$ receptor: GABRA1, GABRA2, GABRA3, GABRA4, GABRA5, GABRA6, GABRB1, GABRB2, GABRB3, GABRG1, GABRG2, GABRG3, GABRD, GABRE, GABRP, GABRQ, GABRR1, GABRR2, GABRR3.

401

402 **Slice preparation for electrophysiology**

403 Coronal slices (300 μm thick) containing the hippocampal region were prepared from mice
404 (at least 8 weeks after xenografting) in accordance with a protocol approved by Stanford
405 University IACUC. After rapid decapitation, the brain was removed from the skull and
406 immersed in ice-cold slicing artificial cerebrospinal fluid (ACSF) containing (in mM): 125
407 NaCl, 2.5 KCl, 25 glucose, 25 $NaHCO_3$ and 1.25 NaH_2PO_4, 3 $MgCl_2$ and 0.1 $CaCl_2$. After
408 cutting, slices were incubated for 30 min in warm (30 °C) oxygenated (95% O2, 5% CO2)
409 recovery ACSF containing (in mM): 100 NaCl, 2.5 KCl, 25 glucose, 25 $NaHCO_3$, 1.25
410 NaH_2PO4, 30 sucrose, 2 $MgCl_2$ and 1 $CaCl_2$ before being allowed to equilibrate at room
411 temperature for an additional 30 min.

412

413 **Electrophysiology**

414 Slices were transferred to a recording chamber and perfused with oxygenated, warmed
415 (28–30 °C) recording ACSF containing (in mM): 125 NaCl, 2.5 KCl, 25 glucose, 25
416 $NaHCO_3$, 1.25 NaH_2PO_4, 1 $MgCl_2$ and 2 $CaCl_2$. NBQX (10 μM) was perfused with the
417 recording ACSF to prevent AMPA receptor-mediated currents in synaptic response
418 experiments. TTX (0.5 μM) was perfused with the recording ACSF to prevent neuronal
419 action potential firing in GABA puff experiments. Slices were visualized using a
420 microscope equipped with DIC optics (Olympus BX51WI). Recording patch pipettes (3-5
421 MΩ) were filled with CsCl-based pipette solution containing (in mM): 150 CsCl, 5 EGTA,
422 1 $MgCl_2$, 10 HEPES, 2 ATP, 0.3 GTP, pH = 7.3. Pipette solution additionally contained
423 Alexa 568 (50 μM) to visualize the cell through dye-filling during whole-cell recordings.

Gramicidin A (60 µg/mL) was added to the pipette solution for perforated patch recordings. Glioma cells were voltage-clamped at −70 mV. Synaptic responses were evoked with a bipolar electrode connected to an Iso-flex stimulus isolator (A.M.P.I.) placed near the xenografted cells. GABA (1 mM) in recording ACSF was applied via a puff pipette, which was placed approximately 100 µm away from the patched cell and controlled by a Picospritzer II (Parker Hannifin Corp.). Optogenetic currents were evoked with a 598 nm LED using a pE-4000 illumination system (CoolLED). Signals were acquired with a MultiClamp 700B amplifier (Molecular Devices) and digitized at 10 kHz with an InstruTECH LIH 8+8 data acquisition device (HEKA). Data were recorded and analyzed using AxoGraph X (AxoGraph Scientific) and IGOR Pro 8 (Wavemetrics). For representative traces, stimulus artifacts preceding the synaptic currents have been removed for clarity. Intracellular chloride concentration was calculated using the Nernst equation.

Inhibitors

Drugs and toxins used for electrophysiology were picrotoxin (50 µM; Tocris), TTX (0.5 µM; Tocris), NBQX (10 µM; Tocris), bumetanide (100 µM), lorazepam (10 µM; Hospira), and levetiracetam (100 µM; Selleck Chemicals). When used for *in vitro* slice application, drugs were made up as a stock in distilled water or dimethylsulfoxide (DMSO) and dissolved to their final concentrations in ACSF before exposure to slices.

Viral injection and fibre optic placement

Animals were anesthetized with 1-4% isoflurane and placed in a stereotaxic apparatus. For optogenetic stimulation experiments, 1 µl of AAV8-Dlx5/6-ChRmine::oScarlet (virus titer= 1.19x1012) (a gift from Dr. Karl Deisseroth from Stanford University; Chen et al., 2020, Nature Biotech) was unilaterally injected using Hamilton Neurosyringe and Stoelting stereotaxic injector over 5 minutes. The viral vector was injected into hippocampus CA1 in the right hemisphere at coordinates: 1.5 mm lateral to midline, -1.8 mm posterior to bregma, -1.3 mm deep to cranial surface. 2 weeks following the viral injection, SU-DIPG-XIII-FL cells were xenografted as described above. After 7 weeks of tumor engraftment, an optic ferrule was placed above the CA1 of the hippocampus of the right hemisphere, at 1.5 mm lateral to midline, -1.8 mm posterior to bregma, -1.25 mm deep to cranial surface.

Optogenetic stimulation

Optogenetic stimulations were performed at least 10 weeks after the viral vector delivery, 8 weeks after xenografts, and 1 week after optic ferrule implantation. Freely moving animals were connected to a 595 nm fiber-coupled LED laser system with a monofiber patch cord. Optogenetic stimulation was performed with cycles of 595 nm light pulses at 40 Hz frequency, 10 ms width, and a light power output of 10-15mW from the tip of the optic fiber, which lasted for 30 seconds, followed by 90 seconds recovery over a 30-minute period. Animals were injected intraperitoneally with 40 mg/kg EdU (5-ethynyl-2'-deoxyuridine; Invitrogen, E10187) before the session, and were perfused 24 hours after the optogenetic stimulations.

469 **Bioluminescence imaging**

470 For in vivo monitoring of tumor growth, bioluminescence imaging was performed using
471 an IVIS imaging system (Xenogen). Mice orthotopically xenografted with luciferase-
472 expressing glioma cells were placed under isofluorane anesthesia and injected with
473 luciferin substrate. Animals were imaged at baseline and randomized based on tumor
474 size by a blinded investigator so that experimental groups contained an equivalent range
475 of tumor sizes. Over the course of each study (described below), all total flux values were
476 then normalized to baseline values to determine fold change of tumor growth.

477

478 **Mouse drug treatment studies**

479 For all drug studies, NSG mice were xenografted as above with SU-DIPG-VI-GFP, SU-
480 DIPG-XIII-FL-GFP, SU-DIPG-50-GFP, SU-pcGBM2-GFP, SF0232, or SF0238 cells and
481 randomized to treatment group by a blinded investigator. Four to six weeks post-
482 xenograft, mice were treated with systemic administration of lorazepam (8 mg kg^{-1} or 2
483 mg kg^{-1}; Hospira), levetiracetam (20 mg kg^{-1}; Selleck Chemicals), or phenytoin (50 mg
484 kg^{-1}; Selleck Chemicals) via intraperitoneal injection, or ethosuximide (300 mg kg^{-1};
485 Selleck Chemicals) via oral gavage for four weeks (5 days per week). For all studies,
486 controls were treated with an identical volume of the relevant vehicle. Bioluminescence
487 imaging was performed before treatment and every 7 days thereafter using an IVIS
488 imaging system (Xenogen) under isoflurane anesthesia. Tumor burden was assessed as
489 fold change in total flux from the beginning to end of treatment.

490

491 **Xenograft survival studies**

For survival studies, morbidity criteria used were either reduction of weight by 15% initial weight, or severe neurological motor deficits consistent with brainstem dysfunction (that is, hemiplegia or an incessant stereotyped circling behavior seen with ventral midbrain dysfunction). Kaplan–Meier survival analysis using log rank testing was performed to determine statistical significance.

Perfusion and immunohistochemistry

Animals were anaesthetized with intraperitoneal avertin (tribromoethanol), then transcardially perfused with 20 ml of PBS. Brains were fixed in 4% PFA overnight at 4 °C, then transferred to 30% sucrose for cryoprotection. Brains were then embedded in Tissue-Tek O.C.T. (Sakura) and sectioned in the coronal plane at 40 µm using a sliding microtome (Microm HM450; Thermo Scientific).

For immunohistochemistry, coronal sections were incubated in blocking solution (3% normal donkey serum, 0.3% Triton X-100 in TBS) at room temperature for 2 hours. Chicken anti-GFP (1:500, Abcam), mouse anti-human nuclei clone 235-1(1:100; Millipore), or rabbit anti-Ki67 (1:500; Abcam) were diluted in antibody diluent solution (1% normal donkey serum in 0.3% Triton X-100 in TBS) and incubated overnight at 4 °C. Sections were then rinsed three times in TBS and incubated in secondary antibody solution containing Alexa 488 donkey anti-chicken IgG, Alexa 594 donkey anti-rabbit IgG, or Alexa 647 donkey anti-mouse IgG used at 1:500 (Jackson Immuno Research) in antibody diluent at 4 °C overnight. Sections were rinsed three times in TBS and mounted with ProLong Gold Mounting medium (Life Technologies).

515

516 **Confocal imaging and quantification of cell proliferation**

517 Cell quantification within xenografts was performed by a blinded investigator using live
518 counting on a 40× oil immersion objective or 20× air objective of a Zeiss LSM700 or Zeiss
519 LSM800 scanning confocal microscope and Zen imaging software (Carl Zeiss). For Ki67
520 analysis, 3 fields for quantification were selected from each of 3 consecutive sections in
521 a 1-in-6 series of 40-μm coronal sections with respect to overall tumor burden. Within
522 each field, all HNA-positive and GFP-positive tumor cells were quantified to determine
523 tumor burden within the areas quantified. HNA-positive were then assessed for co-
524 labelling with Ki67. To calculate the proliferation index (the percentage of proliferating
525 tumor cells for each mouse), the total number of HNA-positive cells co-labelled with Ki67
526 across all areas quantified was divided by the total number of cells counted across all
527 areas quantified (Ki67+/HNA+).

528

529 **EdU Incorporation Assay**

530 Diffuse intrinsic pontine glioma (DIPG) tumor neurosphere cultures SU-DIPGVI, SU-
531 DIPGXIII, and SU-DIPG50 were generated as previously described[3,7] from early post-
532 mortem tissue donations and grown as tumor neurospheres in defined, serum-free 'tumor
533 stem media' (TSM) media, consisting of 1:1 mixture of neurobasal(-A) (Invitrogen) and D-
534 MEM/F-12 (Invitrogen), HEPES buffer (Invitrogen), MEM sodium pyruvate (Invitrogen),
535 MEM non-essential amino acids (Invitrogen), GlutaMAX-1 supplement (Invitrogen), B27(-
536 A) (Invitrogen), human bFGF (20 ng/ml; Shenandoah), human EGF (20 ng/ml;

Shenandoah), human PDGF-AA (10 ng/ml) and PDGF-BB (10 ng/ml; Shenandoah) and heparin (2 ng/ml; Stem Cell Technologies).

100,000 glioma cells were plated onto circular glass coverslips (Electron Microscopy Services) pre-treated for 1 h at 37 °C with poly-L-lysine (Sigma) and then 1 h at 37 °C with 10 µg/ml natural mouse laminin (Thermo Fisher). Dimethyl sulfoxide (Sigma-Aldrich) or drugs at the concentrations indicated (dissolved in dimethyl sulfoxide) were added to the coverslips. 10 µM EdU was added to each coverslip. Cells were fixed after 24 hr using 4% paraformaldehyde in PBS and stained using the Click-iT EdU kit and protocol (Invitrogen). Proliferation index was then determined by quantifying the fraction of EdU labeled cells/DAPI labeled cells using confocal microscopy.

Retrospective, real-world patient data

Retrospective data on patients with high-grade glial tumors were collected from patient databases at Stanford University (1990-2020) and the University of Michigan (2012-2021) through protocols approved by the respective institutional review boards. Database source data for pediatric high-grade glioma patients were reviewed for this study to ensure veracity and completeness. Overall survival was calculated using the Kaplan-Meier estimator; the log-rank test was utilized to compare survival distributions. Patients were censored at time of last contact for the Kaplan-Meier analysis. Given the number of potential parameters with high correlation, an elastic net-regularized regression was utilized for covariate selection in a multivariable survival model. Clinical data including age; sex; tumor location; diagnosis of DMG; and administration of ONC201, panobinostat,

conventional chemotherapy, and levetiracetam were considered potential covariates. Twenty-fold cross-validation was used to obtain the value of λ that gave the minimum mean cross-validated error; corresponding coefficients for each variable were subsequently determined. All data were compiled and analyzed in R version 4.0 or higher.

Statistical analyses

Statistical tests were conducted using Prism (GraphPad) software unless otherwise indicated. Gaussian distribution was confirmed by the Shapiro–Wilk normality test. For parametric data, unpaired two-tailed Student's t-tests or one-way ANOVA with Tukey's post hoc tests to examine pairwise differences were used as indicated. Paired two-tailed Student's t-tests were used in the case of same cell experiments (as in electrophysiological recordings). For non-parametric data, a two-sided unpaired Mann–Whitney test was used as indicated, or a one-tailed Wilcoxon matched-pairs signed rank test was used in the case of same-cell experiments. Two-tailed log rank analyses were used to analyze statistical significance of Kaplan–Meier survival curves. A level of $P < 0.05$ was used to designate significant differences. Based on the variance of xenograft growth in control mice, we used at least three mice per genotype to give 80% power to detect an effect size of 20% with a significance level of 0.05. For all mouse experiments, the number of independent mice used is listed in figure legend. Statistical analyses of retrospective patient data are described above.

Data availability

583 All data are available in the manuscript or from the corresponding author upon reasonable
584 request. Source data will be uploaded with the final version of the manuscript.
585
586 **Code availability**
587 Sources for all code used have been provided, no custom code was created for this
588 manuscript.
589
590 **Acknowledgements:** This work was supported by grants from Cancer Research UK (to
591 M.M.), ChadTough Defeat DIPG (to M.M. and T.B.), the National Institute of
592 Neurological Disorders and Stroke (R01NS092597 to M.M.), NIH Director's Pioneer
593 Award (DP1NS111132 to M.M.), National Cancer Institute (P50CA165962,
594 R01CA258384, U19CA264504 to M.M.), Robert J. Kleberg, Jr. and Helen C. Kleberg
595 Foundation (to M.M.), McKenna Claire Foundation (to M.M.), Kyle O'Connell Foundation
596 (to M.M.), Virginia and D.K. Ludwig Fund for Cancer Research (to M.M.), Waxman
597 Family Research Fund (to M.M.), Will Irwin Research Fund (to M.M.). The authors thank
598 Shawn Hervey-Jumper for the gift of IDH WT adult GBM SF0232 and SF0238 cells.
599
600 **Author contributions:** M.M. and T.B. designed the experiments and wrote the
601 manuscript. T.B., B.Y., K.S. V.M., S.M.J., K.R.T, M.B.K., H.X., M.S., M.A.Q., and P.J.W
602 conducted experiments and performed data analyses. P.G.F., S.P., C.J.C., A.M., C.K.,
603 D.L. maintained patient databases at Stanford and University of Michigan; A.M., E.C.,
604 A.F., S.L., abstracted data from the databases; D.T. and C.K. reviewed source data for
605 all pediatric high-grade glioma database entries to ensure veracity and completeness.

606 All authors contributed to manuscript editing. M.M. conceived the project and

607 supervised all aspects of the work.

608

609 **Author declarations:** M.M. holds equity in MapLight Therapeutics and Syncopation

610 Life Sciences.

611

612
613

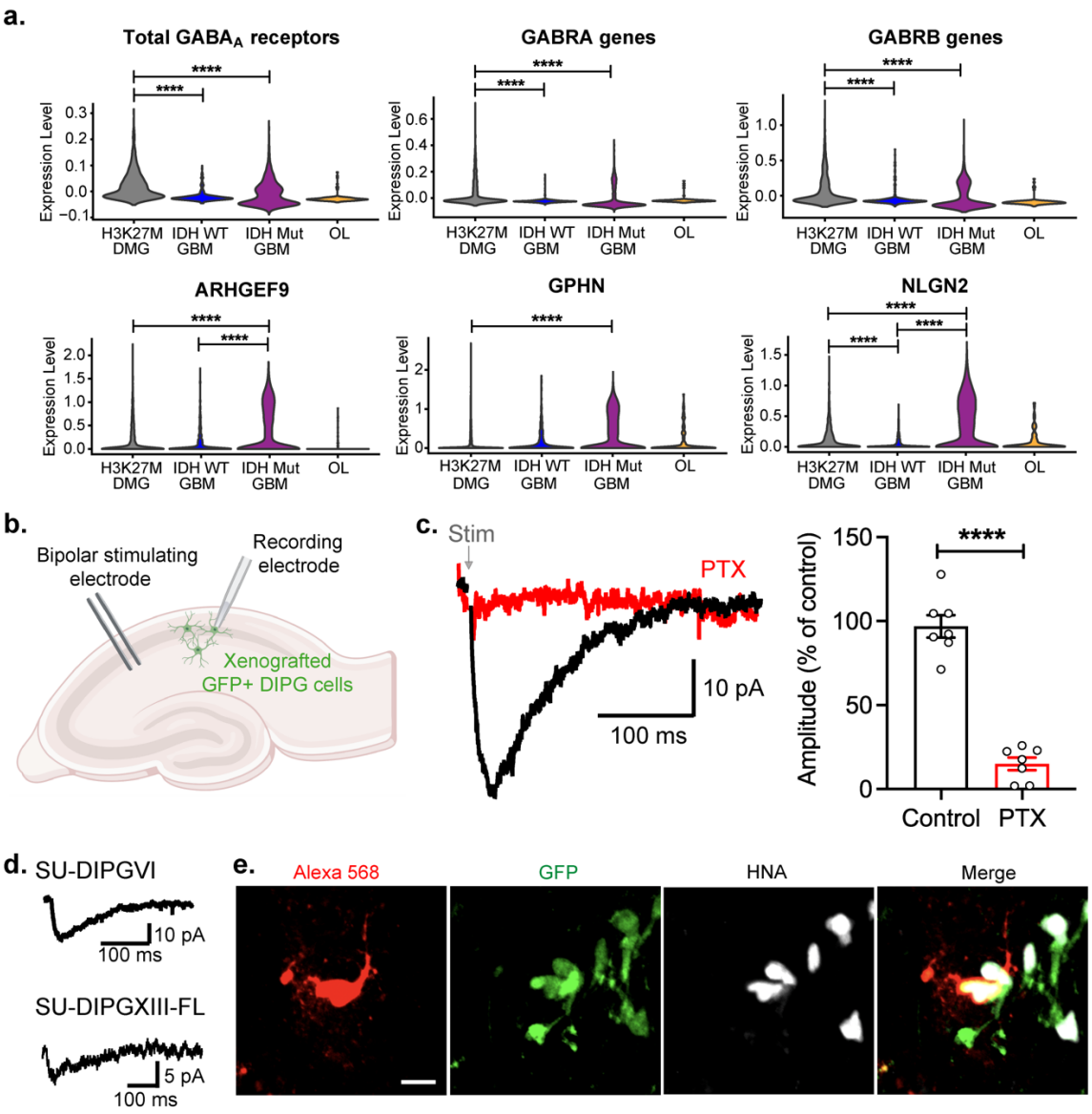

Figure 1. GABAergic neuron-glioma synapses.

a. Single cell RNAseq analysis of primary human biopsies of H3K27M diffuse midline glioma (grey; n = 2,259 cells, 6 study participants), IDH wild-type (WT) high-grade glioma (blue; n = 599 cells, 3 participants), IDH mutant (mut) high-grade glioma (purple; n = 5,096 cells, 10 participants) malignant cells, and tumor-associated, non-malignant oligodendrocytes (OL, yellow; n = 232 cells), demonstrating expression of total $GABA_A$ receptor subunit genes, α subunit genes, β subunit genes, and postsynaptic genes

specific to GABAergic synapses. Statistical analyses performed on single cells are represented with stars only when also significant when analyzed on a per patient basis as well as a per cell basis. Comparisons to OL (control cell type) are not shown.

b. Patient-derived DMG cells expressing GFP were xenografted into the CA1 region of the hippocampus of NSG mice. Response to local CA1 stimulation via a bipolar stimulator was recorded in xenografted cells using whole-cell patch clamp electrophysiology.

c. Representative trace of picrotoxin (PTX)-sensitive GABAergic postsynaptic current (PSC) in a DMG cell (left). Quantification of current amplitude after 50 μM PTX as a % of control (right; n = 7 cells from 5 mice). Recording performed in the presence of NBQX to block AMPAR currents.

d. Representative traces of GABAergic PSCs in two xenografted DMG cell lines.

e. Confocal image of a xenografted DMG cell dye-filled (Alexa 568; red) during recording and co-labelled with GFP (green) and HNA (white) post-recording. Scale bar, 10 μm. All data are mean ± s.e.m. ****P < 0.0001, paired Student's t-test.

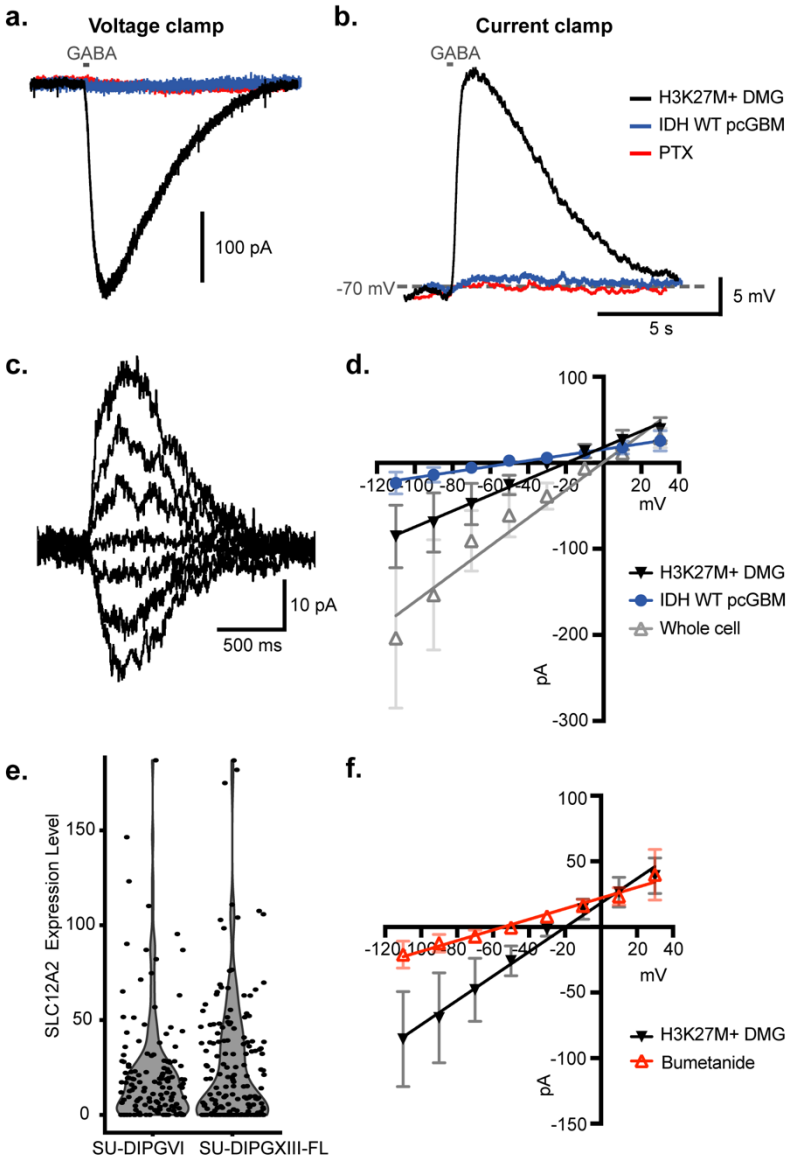

Figure 2. GABA is depolarizing in DMG, but not IDH wild type glioblastoma.

a-b. Perforated patch of xenografted patient-derived H3K27M+ DMG cells and hemispheric (IDH/H3 WT) pediatric cortical glioblastoma (pcGBM) reveals varying current sizes (in voltage clamp, **a.**) and levels of depolarization (in current clamp, **b.**) in response to local GABA application.

c. Representative trace of H3K27M+ DMG cell response to GABA at varying membrane potentials.

d. Current-voltage relationship of GABA current in DMG cells and IDH WT pcGBM cells recorded with perforated patch and whole-cell patch clamp electrophysiology. Reversal potential of GABA was -19.61 mV in H3K27M+ DMG cells (n = 6 cells from 5 mice), -47.44 mV in IDH WT pcGBM cells (n = 6 cells from 5 mice), and -0.4051 mV during whole-cell recording of H3K27M+ DMG cells with a high Cl^- internal solution (n = 4 cells from 4 mice).

e. Single cell RNAseq analysis of SLC12A2 (NKCC1) in patient-derived DMG xenografts.

f. Current-voltage relationship of H3K27M+ DMG cells in the presence of 100 μM bumetanide, a NKCC1 inhibitor. Reversal potential of GABA in DMG cells is -54.20 mV in the presence of bumetanide (n = 5 cells from 3 mice). All data are mean ± s.e.m.

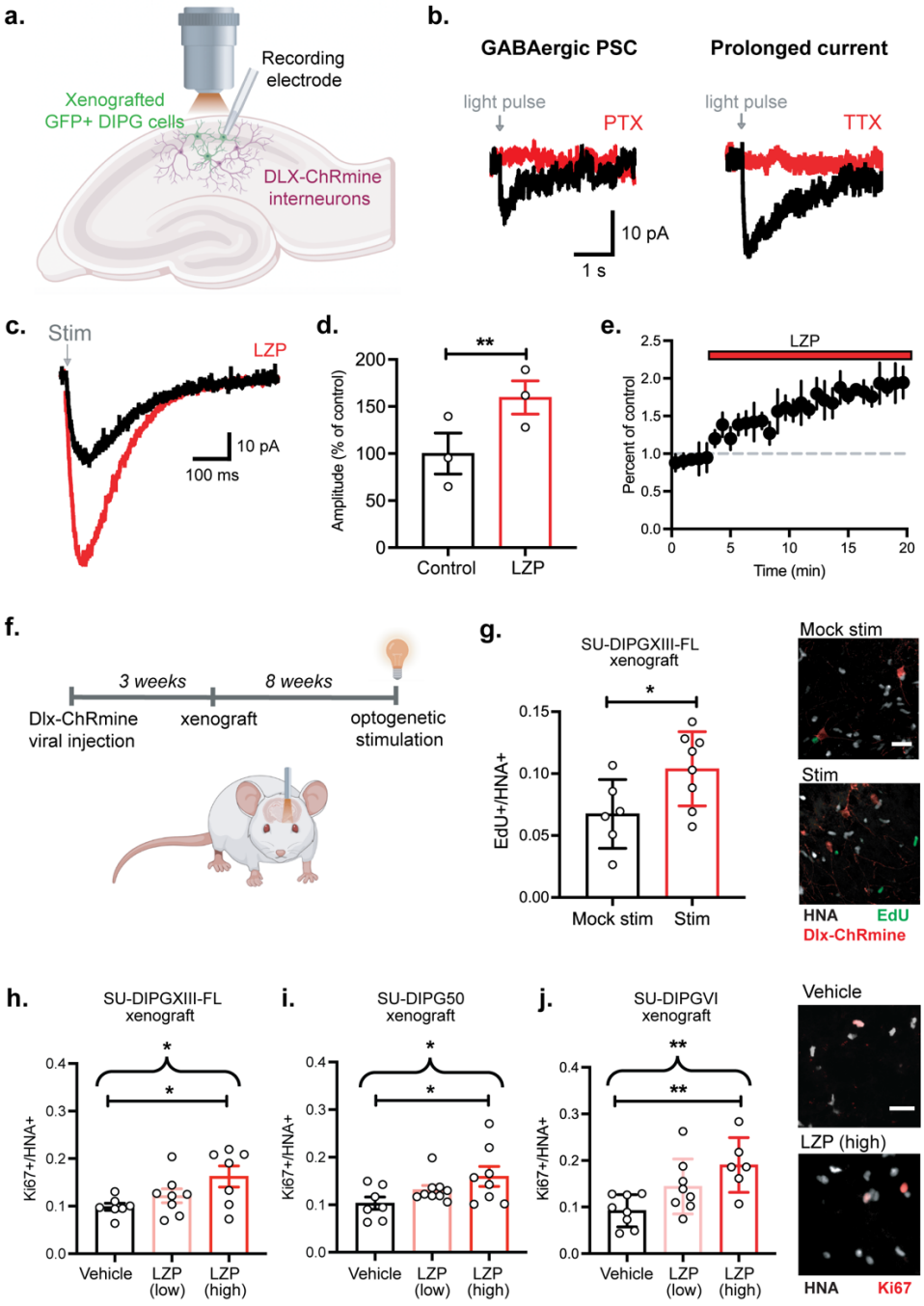

Figure 3. GABAergic interneuron activity drives DMG proliferation.

a. Patient-derived DMG cells expressing GFP were xenografted into the CA1 region of the hippocampus of NSG mice. Response to optogenetic stimulation of GABAergic

interneurons expressing DLX-ChRmine was recorded in xenografted cells using patch clamp electrophysiology.

b. Two types of responses to optogenetic stimulation of GABAergic neurons were recorded in DMG cells: a PTX-sensitive GABAergic PSC (top) and a prolonged tetrodotoxin (TTX)-sensitive current (bottom).

c. Representative trace of GABAergic PSCs in DMG in the absence and presence of 10 μM lorazepam (LZP), a benzodiazepine.

d. Quantification of current amplitude after LZP perfusion as a % of control (n = 3 cells from 3 mice), paired Student's t-test.

e. Time course of GABAergic PSC decrease in response to LZP.

f. Experimental paradigm for *in vivo* optogenetic stimulation of DLX-ChRmine interneurons near xenografted DMG cells in the CA1 region of the hippocampus.

g. Quantification of proliferation index (EdU+/HNA+ cells) after optogenetic stimulation or mock stimulation (left; mock stim, n = 6 mice; stim, n = 8 mice, two-tailed Student's t-test). Right, representative confocal images of DLX-ChRmine GABAergic interneurons (red) near xenografted DMG cells expressing EdU (green) and HNA (white). Scale bar, 25 μm.

h-j. Dose-dependent (low = 2 mg/kg; high = 8 mg/kg) effect of LZP treatment in mice with patient-derived DMG xenografts, SU-DIPGXIII-FL (vehicle, n = 7 mice; low dose, n = 8 mice; high dose, n = 7 mice; **h**), SU-DIPG50 (vehicle, n = 7 mice; low dose, n = 9 mice; high dose, n = 8 mice; **i**), and SU-DIPGVI (vehicle, n = 8 mice; low dose, n = 8 mice; high dose, n = 6 mice; **j**), one-way ANOVA. Straight brackets indicate Dunnett's multiple comparisons test between two groups; curved brackets indicate post-test for linear contrast among all three groups. Right, representative confocal images of xenografted

683 SU-DIPGVI cells expressing Ki67 (red) and HNA (white). Scale bar, 25 μm. All data are

684 mean ± s.e.m. *P < 0.05, **P < 0.01.

685

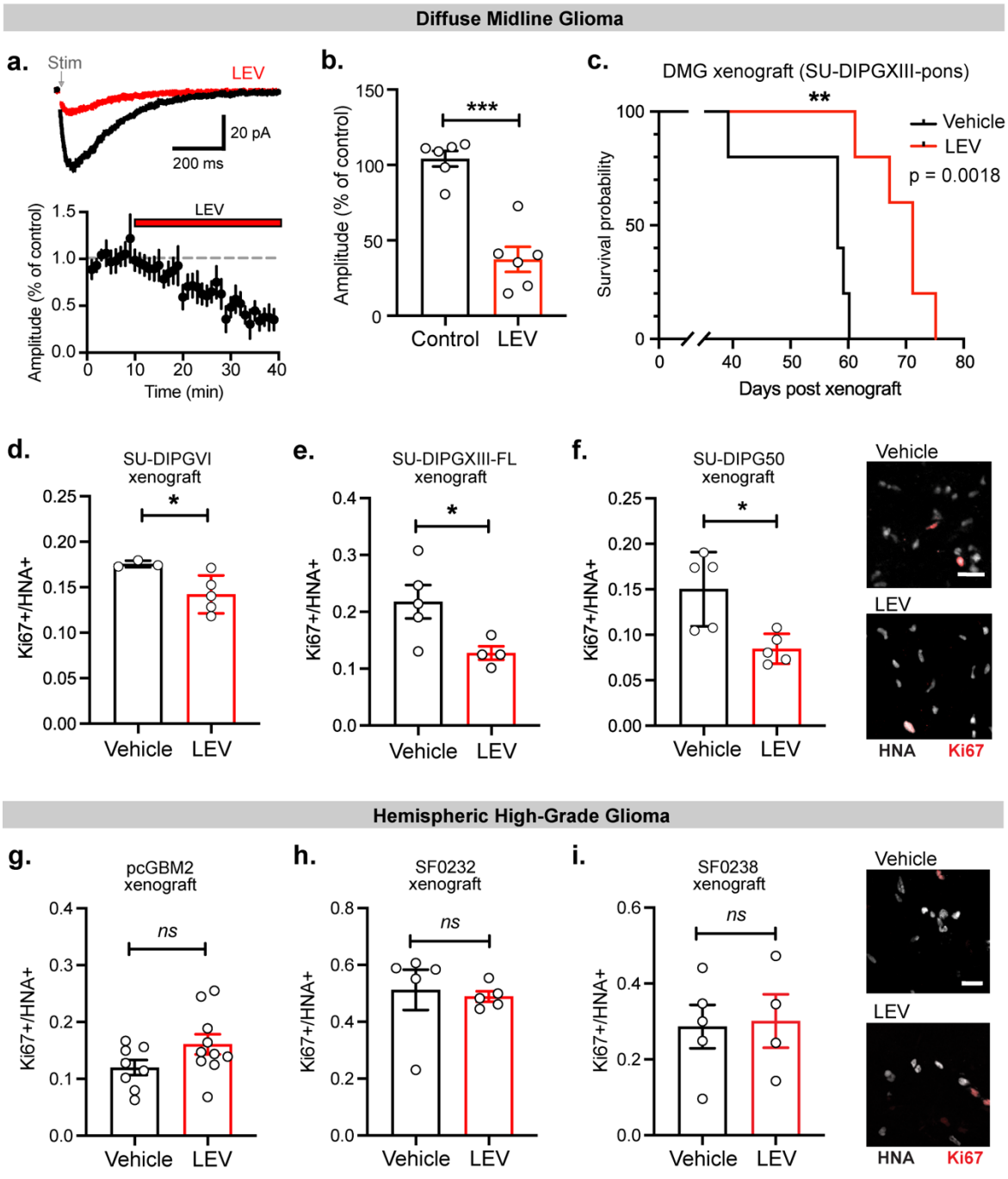

Figure 4. Targeting neuron-to-glioma synapses reduces tumor progression in DMG.

a. Representative trace of GABAergic PSCs in DMG in the absence and presence of 100 µM levetiracetam (LEV), an anti-epileptic drug. Below, time course of GABAergic PSC decrease in response to LEV.

b. Quantification of current amplitude after LEV perfusion as a % of control (n = 6 cells from 5 mice), paired Student's t-test.

c. Kaplan–Meier survival curves of mice with xenografted SU-DIPG-XIII-P tumors treated with LEV or vehicle (n = 5 mice per group).

d-f. Effect of LEV treatment in mice with patient-derived DMG xenografts, SU-DIPGVI (vehicle, n = 3; LEV, n = 5; **d.**), SU-DIPGXIII-FL (vehicle, n = 5 mice; LEV, n = 4 mice; **e.**), and SU-DIPG50 (vehicle, n = 5 mice; LEV, n = 5 mice; **f.**), two-tailed Student's t-test. Right, representative confocal images of xenografted SU-DIPG50 cells expressing Ki67 (red) and HNA (white). Scale bar, 25 µm.

g.-i. No effect of LEV treatment in mice with patient-derived hemispheric high-grade glioma xenografts, pcGBM2 (vehicle, n = 8; LEV, n = 10; **g.**), SF0232 (vehicle, n = 5 mice; LEV, n = 5 mice; **h.**) and SF0238 (vehicle, n = 5 mice; LEV, n = 4 mice), two-tailed Student's t-test. Right, representative confocal images of xenografted SF0238 cells expressing Ki67 (red) and HNA (white). Scale bar, 25 µm. All data are mean ± s.e.m. *P < 0.05, **P < 0.01, ***P < 0.001.

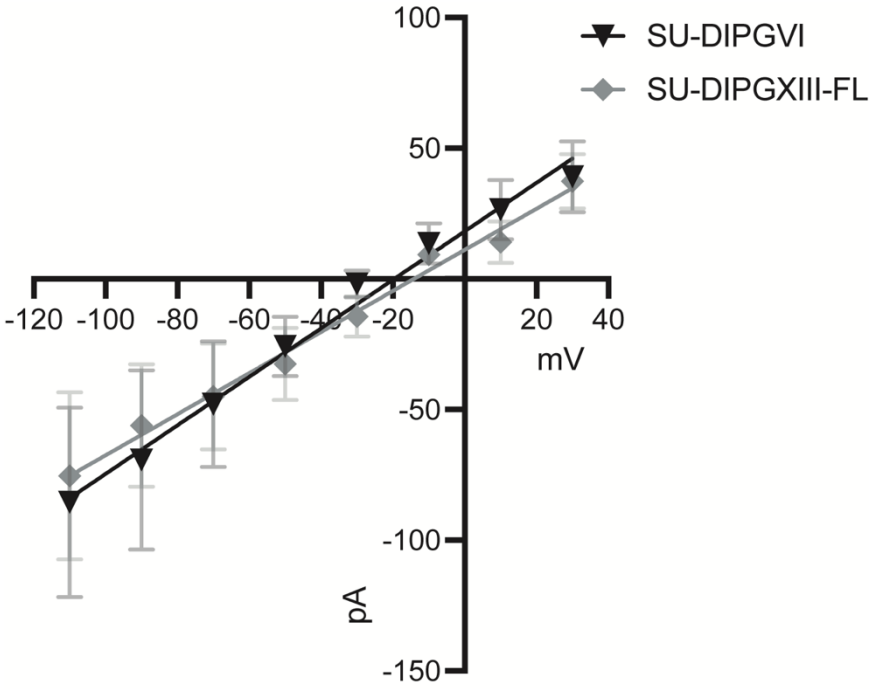

Extended Data Figure 1. Current-voltage relationship of GABA current in two patient-derived DMG xenograft models recorded with perforated patch. Reversal potential of GABA was -19.61 mV in SU-DIPGVI cells (n = 6 cells from 5 mice), and -14.14 mV in SU-DIPGXIII-FL cells (n=5 cells from 3 mice). All data are mean ± s.e.m.

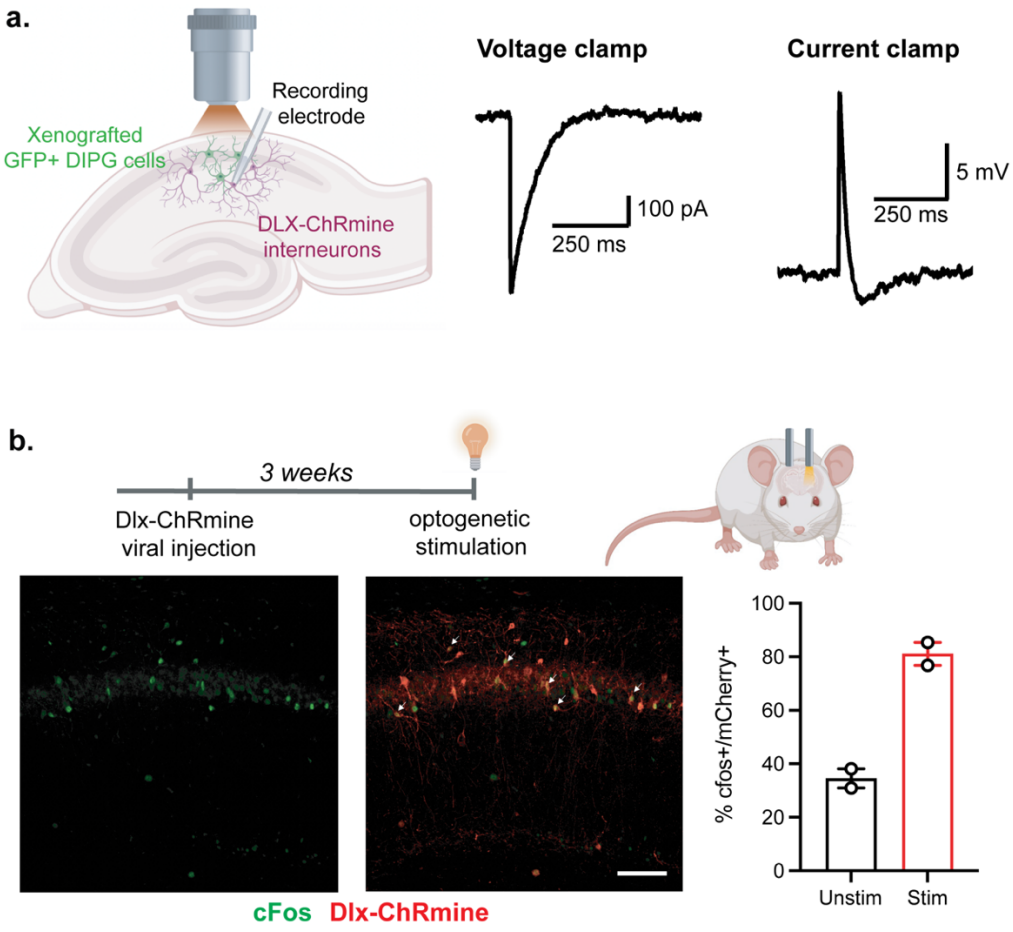

Extended Data Figure 2. Optogenetic stimulation of GABAergic interneurons expressing DLX-ChRmine.

a. Inward current and corresponding depolarization of GABAergic interneurons expressing DLX-ChRmine in response to optogenetic stimulation were recorded in using patch clamp electrophysiology.

b. Optogenetic stimulation of interneurons expressing DLX-ChRmine (red) lead to neuronal activity, indicated by cfos expression (green). Arrows indicate co-labeled cells. Scale bar, 100 μm. Above, experimental timeline. Right, quantification of cfos expression in interneurons in the stimulated hemisphere (stim) is greater than in the unstimulated hemisphere (unstim, n = 2 mice). All data are mean ± s.e.m.

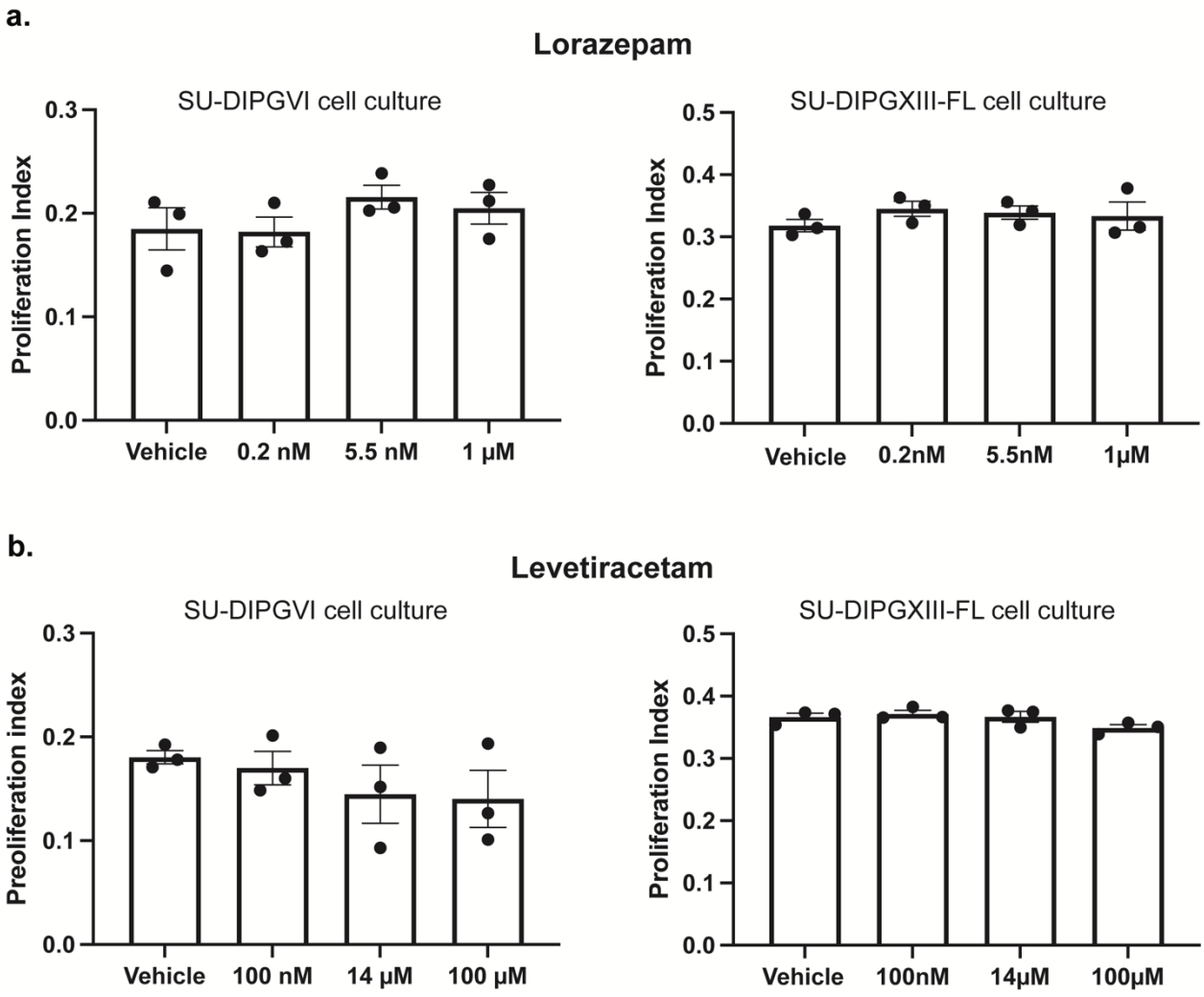

Extended Data Figure 3. Lorazepam and levetiracetam have no effect on proliferation of patient-derived DMG cells in monoculture

a. Lorazepam treatment in patient-derived DMG cultures SU-DIPGVI and SU-DIPGXIII-FL had no effect on proliferation (n = 3 wells per group).

b. Levetiracetam treatment in patient-derived DMG cultures SU-DIPGVI and SU-DIPGXIII-FL had no effect on proliferation (n = 3 wells per group). All data are mean ± s.e.m. Two-tailed Student's t-test.

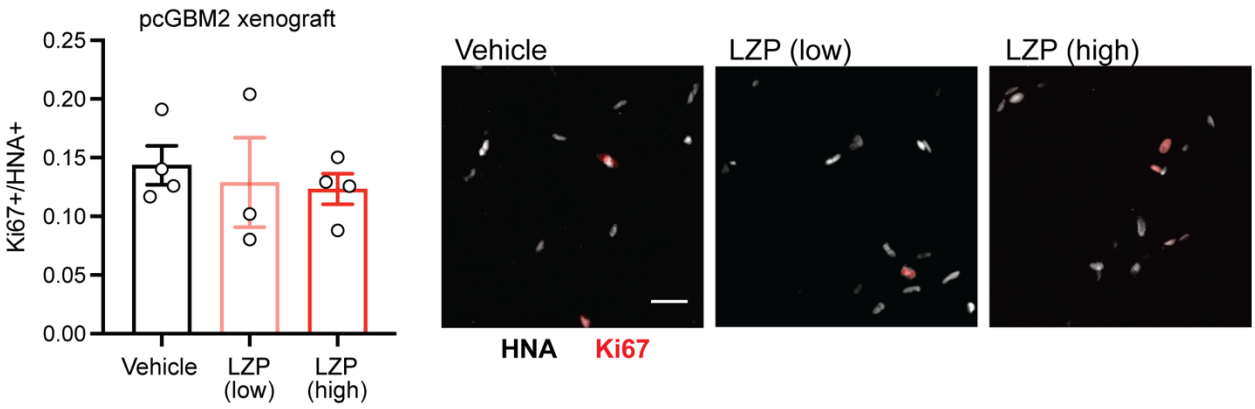

738

739 **Extended Data Figure 4. Lorazepam has no effect on H3/IDH WT pediatric GBM.** LZP
740 treatment in mice with patient-derived pcGBM2 xenografts has no effect on cell
741 proliferation (vehicle, n = 4 mice; low dose, n = 3 mice; high dose, n = 4 mice).
742 Representative confocal images of xenografted pcGBM2 cells expressing Ki67 (red) and
743 HNA (white; right). Scale bar, 25 μm. All data are mean ± s.e.m. One-way ANOVA.

744

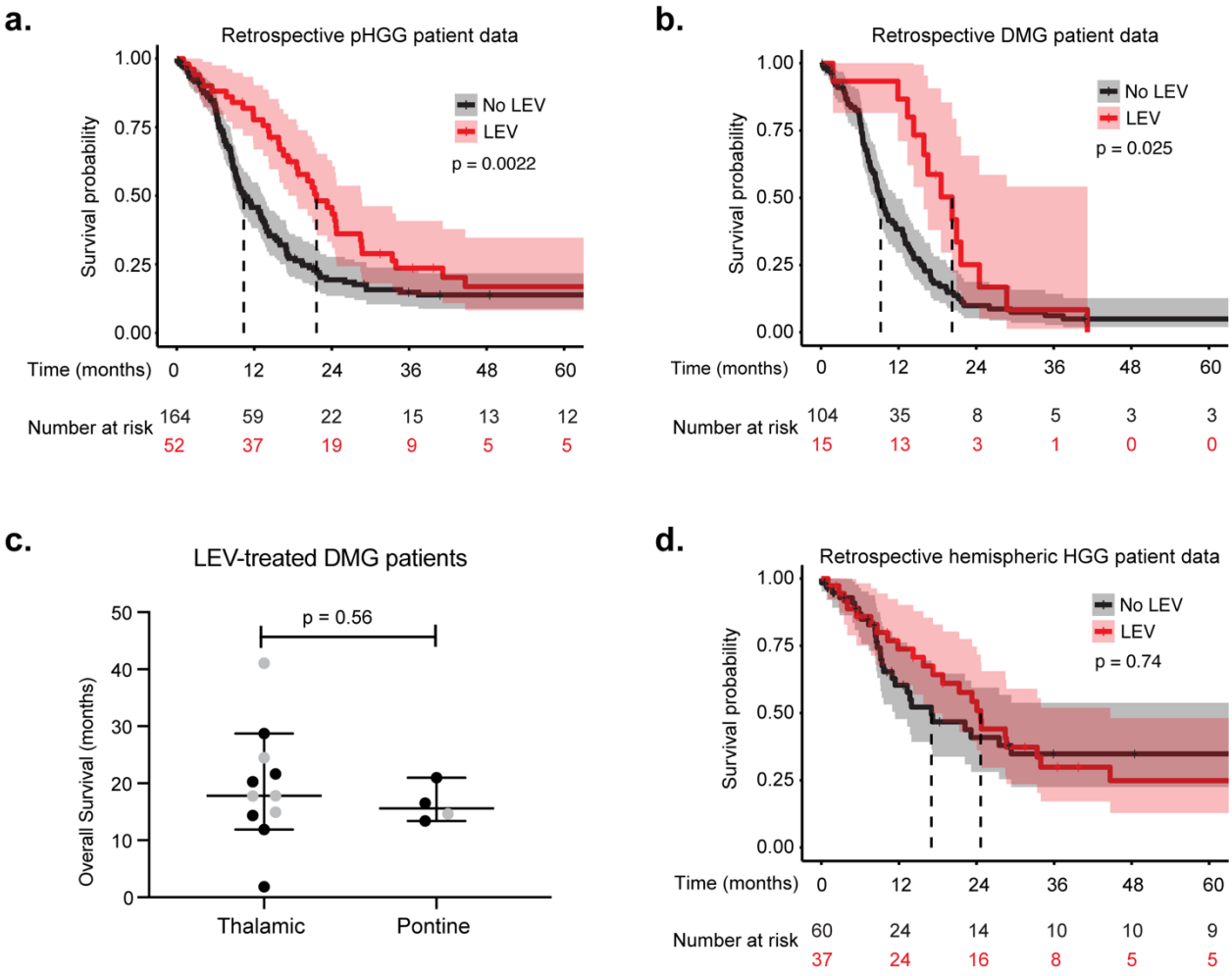

Extended Data Figure 5. Effect of levetiracetam on overall survival in retrospective, real-world patient data.

a. All pediatric high-grade gliomas: Kaplan–Meier overall survival (OS) curves of retrospective data from Stanford University (1990-2020) and University of Michigan (2012-2021) patient databases (n=216), showing pediatric high-grade glioma (pHGG) patients treated with LEV (LEV: median OS = 21.7 months, n = 52; no LEV: median OS= 10.4 months, n = 164).

b. Diffuse midline gliomas: Kaplan–Meier overall survival (OS) curves of retrospective data from DMG patients treated with LEV (LEV: median OS = 20.3 months, n = 15; no LEV: median OS= 9.2 months, n = 105).

c. No difference in overall survival of LEV-treated patients with thalamic compared to pontine DMG (thalamic: n = 11; pontine: n = 4). Grey points are data censored at time of last follow-up. Data are median ± 95% CI. n.s. (P>0.05), two-tailed Student's t-test.

d. Hemispheric high-grade gliomas: Kaplan–Meier overall survival (OS) curves of retrospective data from hemispheric high-grade glioma (HGG) patients treated with LEV (LEV: OS=24.6 months, n = 37; no LEV: OS = 17.0 months, n = 60).

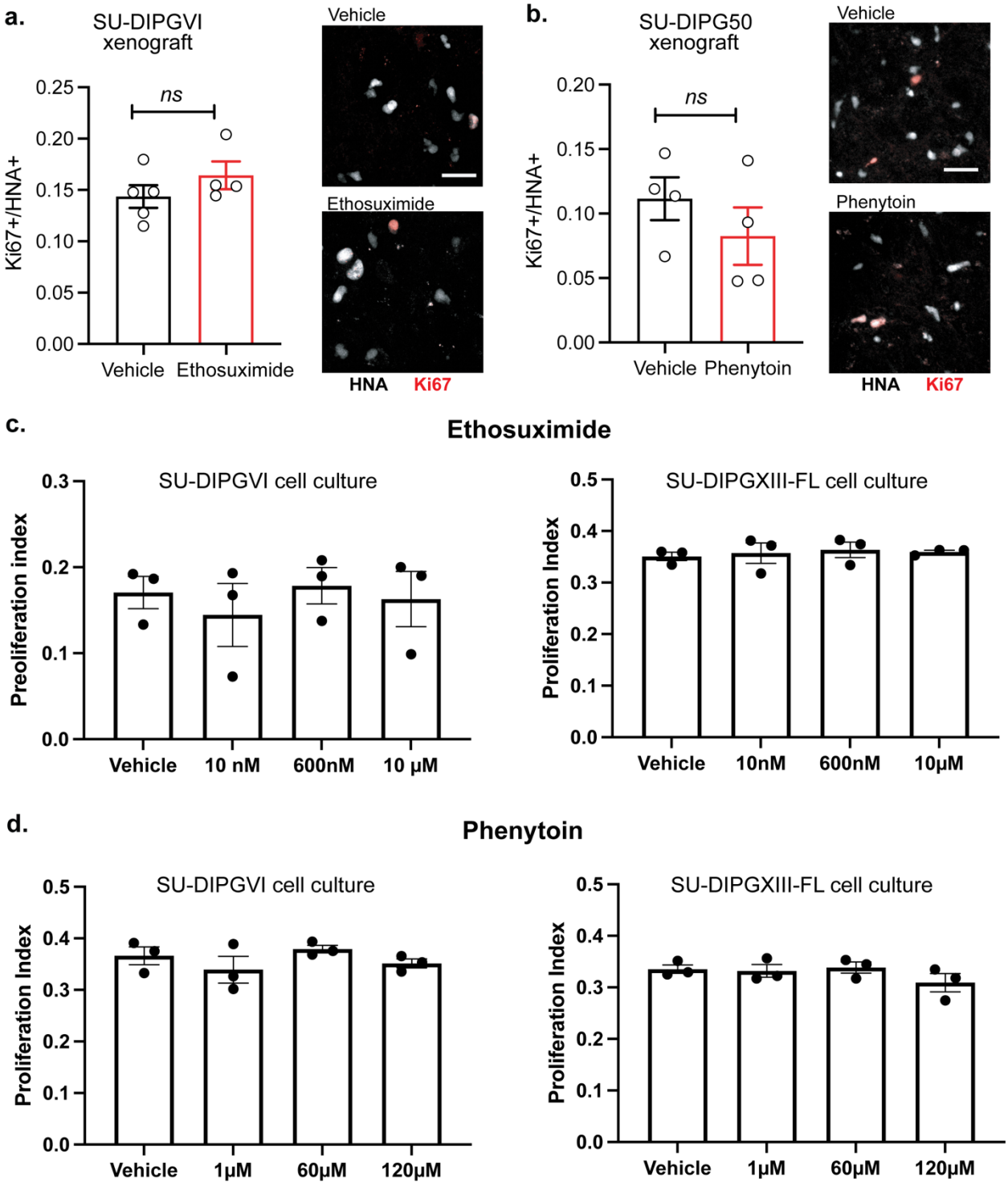

Extended Data Figure 6. Antiepileptic drugs ethosuximide and phenytoin do not affect DMG proliferation.

a. Ethosuximide treatment in mice with patient-derived SU-DIPGVI xenografts has no effect on cell proliferation (vehicle, n = 5 mice; ethosuximide, n = 4 mice). Representative confocal images of xenografted SU-DIPGVI cells expressing Ki67 (red) and HNA (white; right). Scale bar, 25 μm.

b. Phenytoin treatment in mice with patient-derived SU-DIPG50 xenografts has no effect on cell proliferation (vehicle, n = 4 mice; phenytoin, n = 4 mice). Representative confocal images of xenografted SU-DIPG50 cells expressing Ki67 (red) and HNA (white; right). Scale bar, 25 μm.

c. Ethosuximide treatment in patient-derived DMG cultures SU-DIPGVI and SU-DIPGXIII-FL had no effect on proliferation (n = 3 wells per group).

d. Phenytoin treatment in patient-derived DMG cultures SU-DIPGVI and SU-DIPGXIII-FL had no effect on proliferation (n = 3 wells per group). All data are mean ± s.e.m. Two-tailed Student's t-test.

Literature Cited

1 Venkatesh, H. S. *et al.* Neuronal Activity Promotes Glioma Growth through Neuroligin-3 Secretion. *Cell* **161**, 803-816 (2015). https://doi.org:10.1016/j.cell.2015.04.012

2 Pan, Y. *et al.* NF1 mutation drives neuronal activity-dependent initiation of optic glioma. *Nature* **594**, 277-282 (2021). https://doi.org:10.1038/s41586-021-03580-6

3 Venkatesh, H. S. *et al.* Electrical and synaptic integration of glioma into neural circuits. *Nature* **573**, 539-545 (2019). https://doi.org:10.1038/s41586-019-1563-y

4 Venkataramani, V. *et al.* Glutamatergic synaptic input to glioma cells drives brain tumour progression. *Nature* **573**, 532-538 (2019). https://doi.org:10.1038/s41586-019-1564-x

5 Venkataramani, V. T. K., Frank Winkler. Glioblastoma hijacks neuronal mechanisms for brain invasion. *Cell* **in press** (2022).

6 Mackay, A. *et al.* Integrated Molecular Meta-Analysis of 1,000 Pediatric High-Grade and Diffuse Intrinsic Pontine Glioma. *Cancer Cell* **32**, 520-537 e525 (2017). https://doi.org:10.1016/j.ccell.2017.08.017

7 Cooney, T. *et al.* Contemporary survival endpoints: an International Diffuse Intrinsic Pontine Glioma Registry study. *Neuro Oncol* **19**, 1279-1280 (2017). https://doi.org:10.1093/neuonc/nox107

8 Schwartzentruber, J. *et al.* Driver mutations in histone H3.3 and chromatin remodelling genes in paediatric glioblastoma. *Nature* **482**, 226-231 (2012). https://doi.org:10.1038/nature10833

9 Wu, G. *et al.* Somatic histone H3 alterations in pediatric diffuse intrinsic pontine gliomas and non-brainstem glioblastomas. *Nat Genet* **44**, 251-253 (2012). https://doi.org:10.1038/ng.1102 ng.1102 [pii]

10 Khuong-Quang, D. A. *et al.* K27M mutation in histone H3.3 defines clinically and biologically distinct subgroups of pediatric diffuse intrinsic pontine gliomas. *Acta Neuropathol* **124**, 439-447 (2012). https://doi.org:10.1007/s00401-012-0998-0

11 Monje, M. *et al.* Hedgehog-responsive candidate cell of origin for diffuse intrinsic pontine glioma. *Proc Natl Acad Sci U S A* **108**, 4453-4458 (2011). https://doi.org:1101657108 [pii] 10.1073/pnas.1101657108

12 Nagaraja, S. *et al.* Transcriptional Dependencies in Diffuse Intrinsic Pontine Glioma. *Cancer Cell* **31**, 635-652 e636 (2017). https://doi.org:10.1016/j.ccell.2017.03.011

13 Filbin, M. G. *et al.* Developmental and oncogenic programs in H3K27M gliomas dissected by single-cell RNA-seq. *Science* **360**, 331-335 (2018). https://doi.org:10.1126/science.aao4750

14 Nagaraja, S. *et al.* Histone Variant and Cell Context Determine H3K27M Reprogramming of the Enhancer Landscape and Oncogenic State. *Molecular cell* **76**, 965-980 e912 (2019). https://doi.org:10.1016/j.molcel.2019.08.030

15 Haag, D. *et al.* H3.3-K27M drives neural stem cell-specific gliomagenesis in a human iPSC-derived model. *Cancer Cell* **39**, 407-422 e413 (2021). https://doi.org:10.1016/j.ccell.2021.01.005

16 Geraghty, A. C. *et al.* Loss of Adaptive Myelination Contributes to Methotrexate Chemotherapy-Related Cognitive Impairment. *Neuron* **103**, 250-265 e258 (2019). https://doi.org:10.1016/j.neuron.2019.04.032

17 Makinodan, M., Rosen, K., Ito, S. & Corfas, G. A critical period for social experience-dependent oligodendrocyte maturation and myelination. *Science* **337**, 1357-1360 (2012). https://doi.org:10.1126/science.1220845

18 Swire, M., Kotelevtsev, Y., Webb, D. J., Lyons, D. A. & Ffrench-Constant, C. Endothelin signalling mediates experience-dependent myelination in the CNS. *Elife* **8** (2019). https://doi.org:10.7554/eLife.49493

19 Bergles, D. E., Roberts, J. D., Somogyi, P. & Jahr, C. E. Glutamatergic synapses on oligodendrocyte precursor cells in the hippocampus. *Nature* **405**, 187-191 (2000). https://doi.org:10.1038/35012083

20 Lin, S. C. & Bergles, D. E. Synaptic signaling between GABAergic interneurons and oligodendrocyte precursor cells in the hippocampus. *Nat Neurosci* **7**, 24-32 (2004). https://doi.org:10.1038/nn1162

21 Mount, C. W., Yalcin, B., Cunliffe-Koehler, K., Sundaresh, S. & Monje, M. Monosynaptic tracing maps brain-wide afferent oligodendrocyte precursor cell connectivity. *Elife* **8** (2019). https://doi.org:10.7554/eLife.49291

22 Karadottir, R., Cavelier, P., Bergersen, L. & Attwell, D. NMDA receptors are expressed in oligodendrocytes and activated in ischaemia. *Nature* **438**, 1162-1166 (2005). https://doi.org:10.1038/nature04302

23 Kukley, M. *et al.* Glial cells are born with synapses. *FASEB journal : official publication of the Federation of American Societies for Experimental Biology* **22**, 2957-2969 (2008). https://doi.org:10.1096/fj.07-090985

24 Gibson, E. M. *et al.* Neuronal activity promotes oligodendrogenesis and adaptive myelination in the mammalian brain. *Science* **344**, 1252304 (2014). https://doi.org:10.1126/science.1252304

25 Venkatesh, H. S. *et al.* Targeting neuronal activity-regulated neuroligin-3 dependency in high-grade glioma. *Nature* **549**, 533-537 (2017). https://doi.org:10.1038/nature24014

26 Chen, P. *et al.* Olfactory sensory experience regulates gliomagenesis via neuronal IGF1. *Nature* (2022). https://doi.org:10.1038/s41586-022-04719-9

27 Rivera, C. *et al.* The K+/Cl- co-transporter KCC2 renders GABA hyperpolarizing during neuronal maturation. *Nature* **397**, 251-255 (1999). https://doi.org:10.1038/16697

28 Marshel, J. H. *et al.* Cortical layer-specific critical dynamics triggering perception. *Science* **365** (2019). https://doi.org:10.1126/science.aaw5202

29 Robison, N. J. & Kieran, M. W. Diffuse intrinsic pontine glioma: a reassessment. *J Neurooncol* **119**, 7-15 (2014). https://doi.org:10.1007/s11060-014-1448-8

30 Taylor, K. R. *et al.* Glioma synapses recruit mechanisms of adaptive plasticity. *bioRxiv*, 2021.2011.2004.467325 (2021). https://doi.org:10.1101/2021.11.04.467325

31 Labrakakis, C., Patt, S., Hartmann, J. & Kettenmann, H. Functional GABA(A) receptors on human glioma cells. *Eur J Neurosci* **10**, 231-238 (1998).

32 Pallud, J. *et al.* Effect of Levetiracetam Use Duration on Overall Survival of Isocitrate Dehydrogenase Wild-Type Glioblastoma in Adults: An Observational Study. *Neurology* **98**, e125-e140 (2022). https://doi.org:10.1212/WNL.0000000000013005

33 Happold, C. *et al.* Does Valproic Acid or Levetiracetam Improve Survival in Glioblastoma? A Pooled Analysis of Prospective Clinical Trials in Newly Diagnosed Glioblastoma. *J Clin Oncol* **34**, 731-739 (2016). https://doi.org:10.1200/JCO.2015.63.6563

34 Chen, J. S. *et al.* The effect of levetiracetam treatment on survival in patients with glioblastoma: a systematic review and meta-analysis. *J Neurooncol* **156**, 257-267 (2022). https://doi.org:10.1007/s11060-021-03940-2

35 Blanchart, A. *et al.* Endogenous GABAA receptor activity suppresses glioma growth. *Oncogene* **36**, 777-786 (2017). https://doi.org:10.1038/onc.2016.245

36 Tantillo, E. *et al.* Differential roles of pyramidal and fast-spiking, GABAergic neurons in the control of glioma cell proliferation. *Neurobiol Dis* **141**, 104942 (2020). https://doi.org:10.1016/j.nbd.2020.104942

37 Qin, E. Y. *et al.* Neural Precursor-Derived Pleiotrophin Mediates Subventricular Zone Invasion by Glioma. *Cell* **170**, 845-859 e819 (2017). https://doi.org:10.1016/j.cell.2017.07.016

38 Venteicher, A. S. *et al.* Decoupling genetics, lineages, and microenvironment in IDH-mutant gliomas by single-cell RNA-seq. *Science* **355** (2017). https://doi.org:10.1126/science.aai8478

Extended Data Table 1. Diffuse Midline Glioma Patients

Institution	Age (years)	Sex	Diagnosis	Other treatments	Levetiracetam yes/no	Overall survival (days)
University of Michigan	7	Male	Pontine diffuse midline glioma, H3.3K27M, ATRX Q119*, PPM1D G463fs, PDGFRA amplification, KIT, KDR	XRT	Yes	638
University of Michigan	12	Male	Thalamic diffuse midline glioma, H3.3K27M, TP53 H179N, ATRX R2197C, TRIO I780fs deletion, subclonal WAS exon 8 loss, Focal amplifications: HGF, MET, GAB2, TBCD Copy gain NTRK2 (4 copies)	XRT, TMZ, lomustine, Cabozantinib, subtotal resection	Yes	362
University of Michigan	9	Female	Thalamic diffuse midline glioma, H3.1K27M, EGFR A289V, MAX R60Q, PIK3CA R88Q, ARHGAP35 G854E, Subclonal: CEBPZ D78N, DIS3 I779F, MSH3 P64A, BCORL1 K1421fs deletion; subclonal E2F7 L6fs deletion; Copy gain: Chr1q, 2, 5, 7, 15p; UPD: Chr12	XRT, TMZ, Vimpat, ONC201	Yes	659
University of Michigan	13	Female	Thalamic diffuse midline glioma H3K27M, BRAF V600E	XRT, TMZ, Dabrafenib, trametinib, Bevacuzimab, Irinotecan, ONC201, subtotal resection	Yes	Censored at 745
University of Michigan	8	Male	Thalamic diffuse midline glioma, BRAF V600E, H3WT	XRT, Dabrafenib, trametinib, Trileptal, gabapentin, Vimpat	Yes	Censored at 540
University of Michigan	13	Male	Thalamic diffuse midline glioma	XRT, TMZ, ONC201, Oxcarbazine, Zonisamide	Yes	617
University of Michigan	20	Male	Pontine diffuse midline glioma, H3K27M mutant	XRT, TMZ, Depakote, ONC201	Yes	Censored at 446
University of Michigan	10	Female	Thalamic diffuse midline, FBXW R465H, STAG2 R110, SETD2 R2165, VAV1 657A, FGFR3 copy gain, CDK11A/B homozygous deletion, gene fusion FGFR3-PHGDH, FGFR3 copy gain, Gain: chromosomes 1q and 7q; Loss: chromosomes 1p, 4p15-16, 6q, and 10q, H3WT	XRT, COG clinical trial ACNS0831, ponatinib	Yes	Censored at 1249

University of Michigan	10	Male	Thalamic diffuse midline glioma, H3K27M mutation; two TP53 mutations, IDH-1 negative, no MGMT methylation	XRT, ONC201, Bevacizumab, Vimpat, subtotal resection	Yes	Censored at 542
University of Michigan	12	Male	Thalamic diffuse midline glioma, H3K27M mutation; ATRX pR1803H, recurrent (ChrX), NTRK2 internal tandem duplication, focal amplification	XRT, TMZ, ONC201, bevacizumab, entrectinib, subtotal resection	Yes	Censored at 454
Stanford University	6	Female	Pontine diffuse midline glioma	XRT, Etoposide	Yes	407
Stanford University	2	Female	Pontine diffuse midline glioma	XRT	Yes	503
Stanford University	11	Female	Thalamic diffuse midline glioma, H3WT, IDH1/2 WT, ATRX and TP53 mutated	XRT, TMZ, Lomustine, Savolitinib	Yes	874
Stanford University	13	Female	Thalamic diffuse midline glioma, H3K27-altered	NA	Yes	56
Stanford University	11	Male	Thalamic diffuse midline glioma	XRT, TMZ, etoposide	Yes	436
University of Michigan	17	Male	Pontine/spinal diffuse midline glioma, H3.3 K27M, TP53 H179R, ATRX D1313fs, ERCC5 K917fs, Homozygous loss: NF1 Copy loss: BRCA1, CDK12	XRT, SAHA (HDAC inhibitor), subtotal resection	No	316
University of Michigan	5	Female	Pontine diffuse midline glioma, PIK3CA; H3.1 K27M	XRT, everolimus, bevacuzimab, panobinostat, subtotal resection	No	Censored at 588
University of Michigan	13	Male	Pontine diffuse midline glioma, H3.3K27M mutation; FGFR3 activating mutation, loss of BCOR	XRT, bevacizumab, ponatinib, Panobinostat, pazopanib, everolimus subtotal resection	No	Censored at 533
University of Michigan	12	Male	Thalamic diffuse midline glioma, somatic mutations in EGFR V292L, mutation/loss in CDKN2C and BCOR1, EGFR T483_G485del, gene fusion ELF4-SMARCA1, H3WT	Proton XRT, TPCV, Osimertinib, bevacizumab	No	Censored 502
University of Michigan	8	Male	Pontine diffuse midline glioma, H3.3K27M	XRT, COG phase 1 trial (ADVL1217), everolimus, panobinostat, Depakote	No	Censored at 259
University of Michigan	2	Male	Pontine diffuse midline glioma, H3.3K27M, TP53 R273C, CTTNBP2-MET, in frame with MET kinase domain	XRT, cabozantinib	No	Censored at 246

University of Michigan	9	Female	Pontine diffuse midline glioma, H3.3K27M, PPM1D E525, TP53 R248W, additional non-recurrent missense mutations: AFF2 T385N, ABCC1 T826M, PIK3C2G S1183R, PTPRJ E841fs; Copy gain: Chr 1q, 8q, 17q; Loss of Chr11q	Proton XRT, XRT, ONC201	No	
University of Michigan	1	Female	Pontine/thalamic diffuse midline glioma, H3K27M	NA	No	Censored at 29
University of Michigan	7	Female	Pontine diffuse midline glioma, H3.1 K27M, ACVR1 R206H, USP9X splice acceptor, exon33, BCOR A603fs deletion	XRT, ONC201 (arm a), bevacizumab	No	Censored at 626
University of Michigan	13	Male	Thoracic spine diffuse midline glioma, H3.3 K27M, ATRX mutation, FGFR1, H3.3 G34W, PPM1D, PTPN11	XRT, ONC201, bevacizumab, subtotal resection	No	Censored at 398
University of Michigan	17	Female	Thalamic diffuse midline glioma, H3.3, ATRX, PI3KR1, TP53 mutations	Proton XRT, PTC56, ONC201, Subtotal resection	No	Censored at 216
University of Michigan	2	Female	Thalamic diffuse midline glioma, H3K27M	Proton XRT, ONC201	No	Censored at 176
University of Michigan	9	Female	Pontine diffuse midline glioma, H3.3K27M, PDGFA A153T, TP53 P222_E224delinL, IGF1R focal amplification	Proton XRT, ONC201, bevacizumab	No	Censored at 459
University of Michigan	9	Male	Tectal/thalamic diffuse midline glioma, H3K27M mutation, KRAS 212R mutation, HGF amplification	Proton XRT, vincristine, carboplatin, trametinib, ONC201, Subtotal resection	No	Censored at 2220
Stanford University	6	Female	Pontine diffuse midline glioma	XRT, Cisplatin	No	182
Stanford University	16	Male	Pontine diffuse midline glioma	XRT	No	7
Stanford University	5	Male	Pontine diffuse midline glioma	XRT, TMZ, Vorinostat	No	424
Stanford University	7	Male	Pontine diffuse midline glioma	XRT, TMZ	No	50
Stanford University	7	Female	Pontine diffuse midline glioma	XRT, TMZ, Valproic Acid	No	416
Stanford University	15	Male	Pontine diffuse midline glioma	XRT	No	125
Stanford University	9	Male	Pontine diffuse midline glioma	XRT	No	180

Stanford University	13	Male	Pontine diffuse midline glioma, H3.1K27M, MAPKAPK2 gain	XRT, Arsenic Trioxide	No	625
Stanford University	5	Male	Pontine diffuse midline glioma	XRT	No	58
Stanford University	7	Female	Thalamic diffuse midline glioma	XRT, TMZ, Arsenic Trioxide, Bevacizumab, Carmustine, Eroltinib, Irinotecan, Sirolimus, diazepam, phenobarbital, Subtotal Resection	No	1055
Stanford University	9	Female	Pontine diffuse midline glioma	XRT, TMZ	No	231
Stanford University	5	Female	Pontine diffuse midline glioma	XRT	No	110
Stanford University	4	Female	Pontine diffuse midline glioma	XRT, nivolumab	No	Censored at 8
Stanford University	10	Female	Thalamic diffuse midline glioma, H3K27-altered	XRT, TMZ	No	Censored at 1241
Stanford University	4	Female	Pontine diffuse midline glioma	NA	No	116
Stanford University	3	Male	Pontine diffuse midline glioma	NA	No	437
Stanford University	9	Male	Medulla diffuse midline glioma	XRT, TMZ, Bevacizumab, Imetelstat, Carmustine, Subtotal Resection	No	2938
Stanford University	3	Female	Pontine diffuse midline glioma	NA	No	35
Stanford University	8	Female	Pontine diffuse midline glioma	XRT	No	Censored at 53
Stanford University	8	Female	Pontine diffuse midline glioma	XRT	No	281
Stanford University	8	Male	Pontine diffuse midline glioma	XRT	No	197
Stanford University	17	Male	Ponto-medulla diffuse midline glioma	XRT, TMZ, Bevacizumab	No	2324
Stanford University	6	Female	Pontine diffuse midline glioma, H3.3K27M, HIST1H3B gain	XRT	No	54
Stanford University	6	Female	Pontine diffuse midline glioma	NA	No	13
Stanford University	4	Male	Pontine diffuse midline glioma	NA	No	141

Stanford University	6	Male	Pontine diffuse midline glioma	XRT	No	106
Stanford University	4	Male	Pontine diffuse midline glioma	XRT, Arsenic Trioxide	No	205
Stanford University	4	Male	Pontine diffuse midline glioma	XRT	No	397
Stanford University	7	Male	Pontine diffuse astrocytoma (WHO III)	NA	No	58
Stanford University	2	Female	Pontine diffuse midline glioma	NA	No	1140
Stanford University	3	Male	Pontine diffuse midline glioma	XRT	No	487
Stanford University	4	Male	Pontine diffuse midline glioma	XRT	No	196
Stanford University	6	Female	Pontine diffuse midline glioma	XRT	No	223
Stanford University	11	Female	Pontine diffuse midline glioma	XRT, Vorinostat	No	Censored at 201
Stanford University	7	Female	Pontine diffuse midline glioma	XRT	No	Censored at 5
Stanford University	10	Male	Pontine diffuse midline glioma, H3WT	XRT (only 4 doses)	No	66
Stanford University	3	Male	Pontine diffuse midline glioma, H3.1K27M, H3F3A gain, MDM4 gain, ACVR1 point mutation, NTRK1 gain, CDK18 gain, CLK1 gain, CLK2 gain, CLK4 point mutation, NUAK2 gain, STK36 gain, PPP1CB gain, MAPKAPK2 gain	XRT, Rindopepimut, GM-CSF	No	471
Stanford University	11	Male	Pontine diffuse midline glioma	XRT, TMZ, Veliparib	No	484
Stanford University	13	Female	Medulla diffuse midline glioma	XRT, TMZ, Rindopepimut, GM-CSF, imetelstat	No	245
Stanford University	6	Female	Pontine diffuse midline glioma	XRT, TMZ, Rindopepimut, GM-CSF	No	290
Stanford University	8	Male	Cervical glioblastoma (glioblastoma multiforme, astrocytoma WHO IV)	XRT, TMZ, Subtotal Resection	No	894
Stanford University	3	Male	Pontine diffuse midline glioma	XRT	No	Censored at 105
Stanford University	12	Female	Pontine diffuse midline glioma	XRT	No	195

Stanford University	8	Male	Pontine diffuse midline glioma	XRT, Bevacizumab, Imetelstat	No	384
Stanford University	8	Female	Pontine diffuse midline glioma	XRT, cabazitaxel	No	277
Stanford University	9	Female	Pontine diffuse midline glioma, H3K27-altered	NA	No	78
Stanford University	2	Male	Pontine diffuse midline glioma	XRT, cabazitaxel	No	558
Stanford University	4	Female	Pontine diffuse midline glioma, H3K27-altered	XRT, TMZ, Bevacizumab	No	Censored at 645
Stanford University	10	Female	Pontine diffuse midline glioma	XRT, TMZ, ABT-888	Yes (1 dose)	235
Stanford University	5	Male	Pontine diffuse midline glioma	XRT, TMZ, ABT-888	No	183
Stanford University	6	Male	Pontine diffuse midline glioma	XRT,nivolumab x4 doses	No	Censored at 21
Stanford University	6	Female	Pontine diffuse midline glioma, H3K27-altered	XRT, Subtotal resection, antineoplaston	No	515
Stanford University	2	Male	Pontine diffuse midline glioma	XRT, Bevacizumab	No	Censored at 25
Stanford University	14	Female	Spinal diffuse midline glioma, H3K27-altered	Subtotal Resection, XRT, TMZ, intrathecal liposomal cytarabine, panobinostat	No	198
Stanford University	13	Female	Pontine diffuse midline glioma	XRT, panobinostat	No	350
Stanford University	3	Female	Pontine diffuse midline glioma	XRT	No	Censored at 98
Stanford University	16	Male	Pontine diffuse midline glioma	XRT, panobinostat	No	393
Stanford University	6	Female	Pontine diffuse midline glioma	XRT, panobinostat x1 dose	No	266
Stanford University	6	Male	Pontine diffuse midline glioma, H3K27-altered	XRT, TMZ, Subtotal resection, CCNU, pomalidomide, oral cyclophosphamide, oral topotecan	No	395
Stanford University	8	Male	Pontine diffuse midline glioma, H3K27-altered	XRT, panobinostat	No	176
Stanford University	2	Male	Pontine diffuse midline glioma	XRT	No	385

Stanford University	6	Male	Pontine diffuse midline glioma	XRT	No	Censored at 39
Stanford University	7	Male	Pontine diffuse midline glioma, H3K27-altered	XRT	No	185
Stanford University	5	Male	Pontine diffuse midline glioma, H3K27-altered	XRT	No	Censored at 187
Stanford University	10	Male	Pontine diffuse midline glioma	XRT, ONC201	No	190
Stanford University	2	Male	Pontine diffuse midline glioma	XRT	No	462
Stanford University	5	Male	Pontine diffuse midline glioma, H3WT, TP53 loss and point mutation, PDGFR loss, HDAC3 loss, CDK1 gain, CLK4 loss, MAPK7 loss, MYLK loss, TGFBR2 loss, GSK3B loss, PSMB5 gain, PIK3CB loss, HSPBAP1 loss, MDM2 gain, AURKB loss	XRT (only two fractions)	No	217
Stanford University	1	Male	Pontine diffuse midline glioma	XRT, Cisplatin, Cyclophosphamide, Etoposide, Vincristine	No	792
Stanford University	4	Female	Pontine diffuse midline glioma	XRT, Etoposide	No	410
Stanford University	8	Female	Pontine diffuse midline glioma	XRT, Etoposide, Topotecan	No	646
Stanford University	9	Female	Pontine diffuse midline glioma	XRT, TMZ, Etoposide, Thalidomide	No	514
Stanford University	5	Male	Pontine diffuse midline glioma	XRT	No	230
Stanford University	5	Female	Pontine diffuse midline glioma	XRT	No	255
Stanford University	4	Female	Pontine diffuse midline glioma	XRT, Cyclosporine, Etoposide, Vincristine	No	291
Stanford University	5	Female	Pontine diffuse midline glioma	XRT	No	255
Stanford University	4	Male	Pontine diffuse midline glioma	XRT	No	314
Stanford University	6	Female	Pontine diffuse midline glioma	XRT, Cyclosporine, Etoposide, Vincristine	No	222
Stanford University	5	Female	Pontine diffuse midline glioma	XRT, Etoposide, Vincristine	No	295
Stanford University	5	Male	Pontine diffuse midline glioma	XRT, Etoposide	No	305

Stanford University	11	Male	Pontine diffuse midline glioma	XRT, Etoposide, Vincristine	No	115
Stanford University	6	Female	Pontine diffuse midline glioma	XRT, Etoposide, Vincristine	No	218
Stanford University	5	Male	Pontine diffuse midline glioma	XRT, Gadolinium texaphyrin	No	273
Stanford University	4	Female	Pontine diffuse midline glioma	XRT, TMZ	No	190
Stanford University	5	Female	Pontine diffuse midline glioma	XRT, TMZ	No	302
Stanford University	6	Female	Pontine diffuse midline glioma	XRT	No	336
Stanford University	8	Female	Pontine diffuse midline glioma	XRT	No	434
Stanford University	7	Female	Pontine diffuse midline glioma	XRT, Gadolinium texaphyrin	No	353
Stanford University	5	Male	Pontine diffuse midline glioma	XRT	No	160
Stanford University	12	Male	Pontine diffuse midline glioma	XRT	No	Censored at 225
Stanford University	3	Male	Pontine diffuse midline glioma, H3K27-altered	XRT, panobinostat	No	Censored at 427

Legend:
XRT = radiation
TMZ = temozolomide
COG = Children's Oncology Group

Extended Data Table 2. Hemispheric High Grade Glioma Patients

Institution	Age (years)	Sex	Diagnosis	Other treatments	Levetiracetam yes/no	Overall survival (days)
University of Michigan	0.6	Female	Glioblastoma (glioblastoma multiforme, astrocytoma WHO IV), SETD2 S396* mutation, PDGFB amplification (19 copies), H3WT	XRT, TMZ, cisplatin, cyclophosphamide, etoposide, vincristine, dasatinib, Tandem transplant, Subtotal Resection	Yes	871
University of Michigan	16	Male	Cortical/hemispheric astrocytoma, PDGFRA mutant, H3WT	XRT, TMZ, Tripleptal, Vimpat, Dasatanib/Everolimus	Yes	1016
University of Michigan	9	Female	Cortical glioblastoma, TP53 P152L, TP53: Splice donor of exon 4 ATRX R1022* (monoallelic), PRMT2 D95G, Aneuploid CDK4 amplification (chr12; 8 copies), SMARCD1 amplification (chr12; 8 copies), NCOR2 amplification (chr12; 10 copies)	Subtotal resection	Yes	753
University of Michigan	7	Female	Craniopharyngioma (adamantinomatous), CTNNB1 T41I, activating IQGAP3 S1406N	Subtotal Resection	Yes	Censored at 12
University of Michigan	8	Male	Glioblastoma (glioblastoma multiforme, astrocytoma WHO IV), Hypermutation (401.9 Mutations/Mb): TP53 R248W, R158, HDICER1 E1705K, MAP4K3 M1, AMER1 R358*, BCOR R1513*, CTNNA2 R882*, CTNNA1 R451*, IDH1 R100*, KMT2A R407*, PTPN2 R354*, NF1 E2207*, ATM I1581fs, BAX E41fs, FLG E160fs, SOS1 L518fs, NR4A2 Q109fs, KMT2C F835fs, Copy gain chr5 (p15.3-p13.2); Copy loss chr4 (q13.1-q22.1)	XRT, proton XRT, TMZ, bevacuzimab, vorinostat, Valproic acid, cytox, doxorubicin, vincristine, ara-c, methotrexate, pembrolizumab, Subtotal Resection	Yes	3285
University of Michigan	18	Female	Anaplastic pleomorphic xanthoastrocytoma, BRAF V600ETP53 AC276GG, NUTM2F R176G, IRS4 Y828*, PKHD1 A3742V, Genome-wide polyploidy CDKN2A/2B homozygous deletion	Proton XRT, Debrafenib, trametinib, Subtotal Resection	Yes	Censored at 959
University of Michigan	15	Male	Anaplastic astrocytoma, IDH1 R123H-negative, 17.7 Mutations/Mb	Proton XRT, Pembrolizumab, Bevacuzimab, vimpat	Yes	480

			Microsatellite instability (MSI) signature noted TP53 R273C, PTPN11 A72V, PIK3CA Q546R, MITF R110* stopgain, NF1 D2346fs, NF1 G675fs, MSH3 K383fs, WRN E510del, Additional frame-shift mutations: CBX5 K106fs, PDS5B K1318fs, SETD1B H8fs, DDR1 P483fs, TET1 K23fs, SMC5 I939fs, SETD2 N1396fs, TET3 N351fs, copy loss chr14; copy gain chr17q			
University of Michigan	15	Male	Diffuse astrocytoma	XRT, TMZ, Everolimus, Lacosamide	Yes	233
University of Michigan	11	Male	Anaplastic astrocytoma, TP53 I195T, NF1 R440* stopgain, ERBB2 K831T, SCN5A E1060* stopgain, E1070Q, DOCK2 T1279M, ECT2L R233P, Amplifications: Chr3 (CTNNB1, ETV5, SOX2); chr13 (IRS2)	XRT, TMZ, Depakote	Yes	82
University of Michigan	18	Male	Anaplastic astrocytoma (astrocytoma WHO III), ATRX R2178G, PTPN11 Q510L, MYH11 R449Q, E2F1 R166C, POU5F1B R230Q, MYB amplification (exon 1 to 9), Copy loss chr1p-ter, 3p, 2p; UPD chr11p	Vimpat, Gross Total Resection	Yes	Censored at 572
University of Michigan	16	Female	Glioblastoma (glioblastoma multiforme, astrocytoma WHO IV), H3.3 G34R, ATRX E1461* stopgain, GRM3 L91F, PDGFRA P250S, TP53 D186fs insertion, Aneuploidy (polyploidy)	XRT, TMZ, lomustine, Subtotal Resection	Yes	Censored at 309
University of Michigan	18	Male	Anaplastic astrocytoma (astrocytoma WHO III), ATRX S1379* stopgain, NRG3 P289H, CDKN2A/2B deletion, PTPRM deletion, PTPN2 deletion, Copy loss: chr1p, 5q, 11q, 13, 14 UPD: chr17p (TP53), chr4q, 20p	XRT, TMZ, Irinotecan, Palbociclib, Subtotal Resection	Yes	165
University of Michigan	1	Female	Anaplastic astrocytoma (astrocytoma WHO III)	Larotrectinib, Vigabatrin	Yes	Censored at 169
Stanford University	6	Female	Thalamic and medial temporal lobes anaplastic astrocytoma (astrocytoma WHO III)	XRT, TMZ, Lomustine	Yes	277

Stanford University	8	Female	Anaplastic astrocytoma (astrocytoma WHO III)	XRT, TMZ	Yes	404
Stanford University	12	Female	Anaplastic astrocytoma (astrocytoma WHO III)	XRT, TMZ, Topotecan, oral cyclophosphamide (5 days)	Yes	571
Stanford University	11	Female	Glioblastoma (glioblastoma multiforme, astrocytoma WHO IV)	Gross Total Resection	Yes	31
Stanford University	20	Male	Glioblastoma (glioblastoma multiforme, astrocytoma WHO IV)	XRT, TMZ, Bevacizumab	Yes	360
Stanford University	8	Male	Anaplastic astrocytoma (astrocytoma WHO III)	XRT, TMZ, Bevacizumab	Yes	262
Stanford University	15	Male	Glioblastoma (glioblastoma multiforme, astrocytoma WHO IV)	XRT, TMZ, Celocoxib, Lapatinib, Rindopepimut, GM-CSF, Subtotal Resection	Yes	649
Stanford University	7	Male	Glioblastoma (glioblastoma multiforme, astrocytoma WHO IV)	XRT, TMZ, Bevacizumab, Cyclophosphamide, Gross Total Resection	Yes	750
Stanford University	0.1	Female	Glioblastoma (glioblastoma multiforme, astrocytoma WHO IV)	Subtotal resection, TMZ, Carboplatin, Cisplatin, Cyclophosphamide, Eroltinib, Etoposide, Methotrexate, Topotecan, Vincristine, Bevacizumab, Irinotecan	Yes	Censored at 3529
Stanford University	17	Male	Glioblastoma (glioblastoma multiforme, astrocytoma WHO IV)	XRT, TMZ, Bevacizumab	Yes	432
Stanford University	15	Male	Glioblastoma (glioblastoma multiforme, astrocytoma WHO IV)		Yes	Censored at 38
Stanford University	2	Male	Glioblastoma (glioblastoma multiforme, astrocytoma WHO IV), H3WT	Carboplatin, Cisplatin, Cyclophosphamide, Erlotinib, Etoposide, Methotrexate, Topotecan, Vincristine, Gross Total Resection	Yes	Censored at 2504
Stanford University	24	Female	Glioblastoma (glioblastoma multiforme, astrocytoma WHO IV)	XRT, TMZ, Bevacizumab, Cyberknife, Carmustine, Erlotinib, Gross Total Resection	Yes	525
Stanford University	2	Male	Glioblastoma (glioblastoma multiforme, astrocytoma WHO IV)	Subtotal Resection	Yes	107
Stanford University	12	Female	Glioblastoma (glioblastoma multiforme, astrocytoma WHO IV)	XRT, TMZ, Bevacizumab, etoposide, Subtotal Resection	Yes	709
Stanford University	1	Male	Glioblastoma (glioblastoma multiforme, astrocytoma WHO IV)	Carboplatin, Cisplatin, Cyclophosphamide, Eroltinib, Etoposide, Methotrexate,	Yes	Censored at 2284

				Topotecan, Vincristine, Gross Total Resection		
Stanford University	10	Female	Anaplastic astrocytoma (astrocytoma WHO III)	XRT, TMZ, Bevacizumab, Carmustine, Irinotecan	Yes	Censored at 1093
Stanford University	18	Female	Glioblastoma (glioblastoma multiforme, astrocytoma WHO IV)	XRT, TMZ	Yes	122
Stanford University	12	Female	Glioblastoma (glioblastoma multiforme, astrocytoma WHO IV)	XRT, Cisplatin, Cyclophosphamide, Etoposide, Vincristine, cabazitaxel, Subtotal resection	Yes	Censored at 1112
Stanford University	0.3	Male	Glioblastoma (glioblastoma multiforme, astrocytoma WHO IV)	Cisplatin, Cyclophosphamide, Vincristine, topotecan, erlotinib, Gross Total Resection	Yes	Censored at 1210
Stanford University	15	Male	Glioblastoma (glioblastoma multiforme, astrocytoma WHO IV)	XRT, TMZ, CCNU, Bevacizumab, subtotal resection	Yes	732
Stanford University	7	Male	Anaplastic astrocytoma (astrocytoma WHO III)	XRT, TMZ, Bevacizumab, Optune, Irinotecan, Subtotal Resection	Yes	1360
Stanford University	18	Female	Glioblastoma (glioblastoma multiforme, astrocytoma WHO IV)	XRT, TMZ, Bevacizumab, Erlotinib, Near Total Resection	Yes	312
Stanford University	3	Male	Pilocytic astrocytoma (WHO I), relapsed as anaplastic astrocytoma (WHO III)	XRT, TMZ, Bleomycin, P-32, gross total resection	Yes	Censored at 9280
Stanford University	17	Female	Anaplastic astrocytoma (astrocytoma WHO III)	XRT, subtotal resection, TMZ, Bevacizumab, Irinotecan	Yes	1033
Stanford University	11	Female	Anaplastic astrocytoma (astrocytoma WHO III)	XRT, TMZ, Etoposide, Irinotecan, Oxaliplatin, Subtotal Resection	Yes	866
Stanford University	0.4	Female	Glioblastoma (glioblastoma multiforme, astrocytoma WHO IV), H3WT	Antineoplastons, etoposide, Bevacizumab, Gross Total Resection	Yes	Censored at 432
Stanford University	20	Female	Glioblastoma (glioblastoma multiforme, astrocytoma WHO IV)	XRT, TMZ, Gross Total Resection	Yes	Censored at 70
University of Michigan	14	Male	Right Parietal Glioblastoma Multiforme, somatic TSC2 R611W mutation, homozygous deletion of PAK1, germline loss of TP53	Proton XRT, everolimus, Gross total resection	No	Censored at 1953
University of Michigan	16	Female	Glioblastoma multiforme, PDGFRRA V536E and P577R, STAG2 R263W	XRT, dasatinib, etoposide, subtotal resection	No	Censored at 203
University of Michigan	15	Male	Pleomorphic, xanthoastrocytoma, grade 2, BRAF V600E positive	Proton XRT, subtotal resection	No	Censored at 836
University of Michigan	7	Female	Anaplastic ependymoma, PF-EPN-A, 1q and 5p gain	Proton XRT, Gross total resection	No	Censored at 811

Stanford University	20	Male	Anaplastic astrocytoma (astrocytoma WHO III)	XRT, Carboplatin, Lomustine, Procarbazine, Vincristine	No	417
Stanford University	10	Male	Anaplastic astrocytoma (astrocytoma WHO III)	XRT, TMZ, Etoposide, Thalidomide, Subtotal Resection	No	252
Stanford University	0.8	Male	Glioblastoma (glioblastoma multiforme, astrocytoma WHO IV)	Etoposide, Subtotal Resection	No	146
Stanford University	16	Male	Anaplastic astrocytoma (astrocytoma WHO III)	XRT, TMZ, Subtotal Resection	No	Censored at 57
Stanford University	17	Male	Glioblastoma (glioblastoma multiforme, astrocytoma WHO IV)	XRT, TMZ, Oxaliplatin, Subtotal Resection	No	Censored at 386
Stanford University	15	Female	Glioblastoma (glioblastoma multiforme, astrocytoma WHO IV)	XRT, TMZ, Subtotal Resection	No	Censored at 61
Stanford University	2	Female	Anaplastic astrocytoma (astrocytoma WHO III)	Gross Total Resection	No	Censored at 26
Stanford University	17	Female	Anaplastic astrocytoma (astrocytoma WHO III), H3WT	XRT, Subtotal Resection	No	Censored at 411
Stanford University	4	Male	Anaplastic astrocytoma (astrocytoma WHO III)	Gross Total Resection	No	Censored at 32
Stanford University	9	Female	Glioblastoma (glioblastoma multiforme, astrocytoma WHO IV)	XRT, TMZ	No	25
Stanford University	14	Male	Glioblastoma (glioblastoma multiforme, astrocytoma WHO IV)	XRT, TMZ, Lomustine, Subtotal Resection	No	285
Stanford University	0	Male	Glioblastoma (glioblastoma multiforme, astrocytoma WHO IV)	TMZ, Lomustine, Subtotal Resection	No	Censored at 17
Stanford University	17	Female	Thalamic glioblastoma (glioblastoma multiforme, astrocytoma WHO IV)	XRT, TMZ, Lomustine, Bevacizumab	No	837
Stanford University	16	Female	Glioblastoma (glioblastoma multiforme, astrocytoma WHO IV)	XRT, TMZ, Carboplatin, Cisplatin, Cyclophosphamide, Vincristine, Bevacizumab, Irinotecan, Subtotal Resection	No	Censored at 2067
Stanford University	13	Female	Posterior fossa glioblastoma (glioblastoma multiforme, astrocytoma WHO IV)	XRT, TMZ, Bevacizumab, Imatinib mesylate	No	523
Stanford University	11	Female	Glioblastoma (glioblastoma multiforme, astrocytoma WHO IV)	XRT, TMZ, Bevacizumab, Subtotal Resection, BCNU, irinotecan	No	705
Stanford University	10	Male	Glioblastoma (glioblastoma multiforme, astrocytoma WHO IV)	XRT, TMZ, Bevacizumab, Cediranib, Carmustine, Irinotecan, Gross Total Resection	No	518
Stanford University	9	Female	Pontine and cerebellar anaplastic astrocytoma (astrocytoma WHO III)	XRT, Arsenic Trioxide	No	Censored at 220

Stanford University	11	Female	Glioblastoma (glioblastoma multiforme, astrocytoma WHO IV)	XRT, TMZ, Arsenic Trioxide, Bevacizumab, Irinotecan, Cyclophosphamide, subtotal resection	No	424
Stanford University	16	Male	Anaplastic astrocytoma (astrocytoma WHO III), H3WT	XRT, TMZ, Subtotal Resection	No	Censored at 3893
Stanford University	6	Male	Glioblastoma (glioblastoma multiforme, astrocytoma WHO IV)	NA	No	Censored at 12
Stanford University	0	Female	Glioblastoma (glioblastoma multiforme, astrocytoma WHO IV)	Subtotal Resection	No	1
Stanford University	11	Female	Anaplastic astrocytoma (astrocytoma WHO III)	XRT, TMZ, Bevacizumab, Etoposide	No	258
Stanford University	9	Male	Glioblastoma (glioblastoma multiforme, astrocytoma WHO IV)	XRT, TMZ, Bevacizumab	No	333
Stanford University	9	Female	Glioblastoma (glioblastoma multiforme, astrocytoma WHO IV)	XRT, TMZ, Bevacizumab, Lomustine, Gross Total Resection	No	Censored at 331
Stanford University	7	Female	Thalamic anaplastic astrocytoma (astrocytoma WHO III)	XRT, TMZ, Carboplatin, Vincristine	No	Censored at 308
Stanford University	2	Female	Glioblastoma (glioblastoma multiforme, astrocytoma WHO IV), H3WT	XRT, TMZ, Vorinostat, Gross Total Resection	No	Censored at 556
Stanford University	11	Female	Diffuse astrocytoma (astrocytoma WHO II)	Gross Total Resection	No	Censored at 1475
Stanford University	4	Female	Anaplastic astrocytoma (astrocytoma WHO III)	Gross Total Resection	No	Censored at 4830
Stanford University	9	Female	Anaplastic astrocytoma (astrocytoma WHO III)	XRT, TMZ, Lomustine	No	Censored at 249
Stanford University	*in utero* (at 36-week ultrasound)	Female	Glioblastoma (glioblastoma multiforme, astrocytoma WHO IV), H3WT, IDH WT	Etoposide, Carboplatin, Cyclophosphamide, Vincristine	No	Censored at 883
Stanford University	5	Female	Glioblastoma (glioblastoma multiforme, astrocytoma WHO IV), H3K27-altered		No	Censored at 161
Stanford University	2	Male	Mixed malignant germ cell tumor	XRT, Carboplatin, Etoposide, Ifosfamide, Subtotal Resection	No	187
Stanford University	0.6	Male	Anaplastic astrocytoma (astrocytoma WHO III)	Subtotal Resection	No	Censored at 30
Stanford University	0.7	Female	Glioblastoma (glioblastoma multiforme, astrocytoma WHO IV), H3WT	Cisplatin, Cyclophosphamide, Methotrexate, Vincristine	No	Censored at 262

Stanford University	11	Female	Anaplastic ependymoma	XRT, Carboplatin, Cyclophosphamide, Etoposide, Vincristine	No	Censored at 107
Stanford University	2	Female	Anaplastic astrocytoma (astrocytoma WHO III), H3WT	Carboplatin, Vinblastine, Vincristine	No	Censored at 281
Stanford University	7	Female	Anaplastic astrocytoma (astrocytoma WHO III)	XRT, Cisplatin	No	176
Stanford University	6	Male	Anaplastic astrocytoma (astrocytoma WHO III)	XRT, Cisplatin, Subtotal Resection	No	157
Stanford University	9	Male	Glioblastoma (glioblastoma multiforme, astrocytoma WHO IV)	Carmustine, Etoposide, 6-thioguanine, Subtotal Resection	No	86
Stanford University	5	Female	Anaplastic astrocytoma (astrocytoma WHO III)	XRT, Carboplatin, Etoposide, Ifosfamide	No	Censored at 308
Stanford University	10	Male	Glioblastoma (glioblastoma multiforme, astrocytoma WHO IV)	XRT, TMZ, Celocoxib, Subtotal Resection	No	Censored at 53
Stanford University	13	Male	Glioblastoma (glioblastoma multiforme, astrocytoma WHO IV)	XRT, Lomustine, Procarbazine, Vincristine, Etoposide, Subtotal Resection	No	894
Stanford University	17	Female	Glioblastoma (glioblastoma multiforme, astrocytoma WHO IV)	XRT, TMZ, Carmustine, Imatinib mesylate	No	676
Stanford University	17	Female	Glioblastoma (glioblastoma multiforme, astrocytoma WHO IV)	XRT, TMZ	No	293
Stanford University	14	Male	Glioblastoma (glioblastoma multiforme, astrocytoma WHO IV)	XRT, TMZ, Lomustine, Procarbazine, Vincristine, Thalidomide, Subtotal Resection	No	1993
Stanford University	12	Female	Glioblastoma (glioblastoma multiforme, astrocytoma WHO IV)	XRT, Lomustine, Procarbazine, Vincristine, Gross Total Resection	No	Censored at 4976
Stanford University	4	Male	Glioblastoma (glioblastoma multiforme, astrocytoma WHO IV)	Subtotal Resection	No	51
Stanford University	13	Male	Astrocytoma (anaplastic vs pleomorphic xanthoastrocytoma)	XRT, TMZ, Gross Total Resection	No	Censored at 3007
Stanford University	7	Female	Anaplastic astrocytoma (astrocytoma WHO III)	XRT, Carmustine, Cisplatin, Topotecan, Subtotal Resection	No	347
Stanford University	1	Female	Anaplastic astrocytoma (astrocytoma WHO III)	XRT, TMZ, Thalidomide	No	3852
Stanford University	2	Female	Gliosarcoma	XRT, Carmustine, O-6-benzylguanine, Subtotal Resection	No	222
Stanford University	8	Female	Anaplastic astrocytoma (astrocytoma WHO III)	XRT, TMZ, Carmustine, O-6-benzylguanine	No	279

Stanford University	2	Male	Diffuse astrocytoma (WHO II), then glioblastoma (glioblastoma multiforme, astrocytoma WHO IV)	XRT, TMZ, Subtotal Resection, bevacizumab, regorafenib, palbociclib, savolitinib	No	6957
Stanford University	7	Male	Anaplastic astrocytoma (astrocytoma WHO III)	XRT, TMZ, Imatinib mesylate, Subtotal Resection	No	263

Legend:
XRT = radiation
TMZ = temozolomide